SCHOOL OF ENGINEERING AND DESIGN

TECHNICAL UNIVERSITY OF MUNICH

Master's Thesis

Automatically evaluating road safety of cyclists using semantic 3D city models

Author:	Shota Yamamoto
Supervisors:	Dr. Ihab Hijazi
	M.Sc. Christof Beil
	Dr.-Ing. Andreas Donaubauer
External Supervisor:	M.Sc. Felix Rauch, DLR
Advisors:	Univ.-Prof. Dr. rer. nat. Thomas H. Kolbe
Submission Date:	20.10.2025

Abstract

This thesis presents a systematic framework for three-dimensional visibility analysis to assess cyclists' safety at urban intersections using CityGML 3.0 and parking area data extracted using AI-based models trained on the TIAS dataset. Unlike previous visibility studies that are mostly motorist-centric and limited to static or local analyses, this research introduces a scalable, data-driven, and semantically informed methodology that incorporates the geometric and semantic data use of modern 3D city models. The framework overcomes recurring limitations in existing studies by automating visibility quantification and integrating roadside parking data from TIAS into CityGML. The data derived from these datasets represent real-world obstructions with high geometrical accuracy and semantic information.

The analysis proposes systematical evaluations of intervisibility between cyclists and drivers across multiple intersections within two study areas in Munich, considering the influence of urban elements such as buildings, vegetation, city furniture, and parked vehicles. Through this approach, the thesis demonstrates how semantic 3D city datasets can enhance reproducibility and scalability in urban visibility studies. The results highlight the applicability of the proposed framework for city-wide assessments, supporting evidence-based and cyclist-inclusive urban design and traffic safety planning.

Contents

1 Introduction

1.1 Background

Germany has been investing in the development of cycling infrastructure for decades and is now one of the countries with an extensive network of cycling routes. People's awareness of environmental protection and the health benefits cycling brings is high. A rise in cycling popularity is reflected in data showing a 40% increase between 1996 and 2018, as reported by Hudde (2022). However, despite the popularity of cycling in Germany, the number of collisions involving cyclists that result in injury or death remains high, indicating that it is still a risky mode of transport [Harkort et al. (2023)]. The vulnerability of cyclists is attributable to factors such as slower speeds, no licensing obligation, and lower adherence to traffic rules, as well as the road design, which requires cyclists to share road space with motorized vehicles, thereby increasing the risks for cyclists [Harkort et al. (2023)]. With many conflict points between cyclists and motorized vehicles present in urban environments due to the factors above, lack of visibility is the primary direct cause for car drivers to overlook the presence of cyclists and other vulnerable road users (VRU) on the road [González-Gómez et al. (2021)]. Urban streets have many elements that can block the view of road users, such as buildings, vegetation, parked vehicles, traffic signs, and overpasses, in addition to road geometries. These characteristics in urban environments collectively increase the risk of collisions between cyclists and motorized vehicles. It is important to investigate crush-prone areas in terms of visibility. Visibility investigations on the road are essential when building a new road, redesigning an existing one, and integrating new roadside elements to ensure sufficient visible distance, as stipulated in many countries' road design regulations. The commonly employed method is sight distance analysis, utilizing spatial analysis tools such as Line of Sight, as discussed in more detail in the literature and methodology section. However, the existing studies primarily focus on visibility from the perspective of motorists, and few target cyclists and pedestrians (vulnerable road users, or VRUs). There are, in fact, many studies focusing on the safety of cyclists, but their primary approach is limited to psychological and perceptual factors. That is, visibility analysis for cyclists using spatial data is not yet established as a common approach, in contrast to the significant amount of research conducted targeting motorists.

1.2 Research Question

With the increasing availability of 3D city data, road visibility research has undergone significant evolution, leveraging digital representations such as CityGML and LiDAR-derived datasets. These data formats offer great potential for analyzing cyclists' visibility in urban environments, as they can accurately replicate roads and surrounding infrastructure, thus supporting realistic 3D simulation-based analyses. The primary goal of this thesis is to conduct a 3D spatial analysis of bicycle visibility in urban environments, using Munich as the case study area. This choice was due to the availability of a lane-level CityGML dataset from the Chair of Geoinformatics and the the parking area segmentation data derived from TIAS (Traffic Infrastructure and Surroundings) dataset provided by DLR (German Aerospace Center), hereafter referred to as the TIAS segmentation results. The study examines the reciprocal visibility between cyclists and motorists in various urban traffic scenarios, with particular emphasis on visibility conditions at intersections. The reason for this focus the higher frequency of accidents involving vulnerable road users (VRUs) at intersections [Ding et al. 2021], highlighting opportunities for improving road safety. The analyses were conducted using ArcGIS geoprocessing tools, specifically the Line of Sight (LoS) and Intervisibility tools. Four research questions guide the study:

- What are the key steps to develop an automated visibility analysis to assess cyclists' safety in urban intersections?
- To what extent do CityGML and TIAS data provide a practical foundation for conducting 3D visibility analysis in urban environments?
- Can a scalable approach for visibility analysis be developed to enable city-wide assessments?
- How can roadside parking data in the TIAS-based dataset be integrated into CityGML?

These questions are formulated around the novelty and potential of CityGML data, particularly the Transportation Module, which serves as the foundation for the visibility analysis.

1.3 Thesis Structure

The following part of the thesis is structured as follows: Chapter 2 reviews the existing literature on bicycle safety, visibility analysis, intersection designs, and the use of 3D urban models, identifying methodological and technical gaps. Chapter 3 outlines the conceptual and methodological framework, including data sources, scenario design, study areas, and analytical approaches for different collision patterns. Chapter 4 details the implementation

process, describing data preprocessing, model development, and the setup of the visibility analyses. Chapter 5 presents the results of the analyses and examines the performance of the constructed models. Chapter 6 discusses the findings in the context of scalability, data evaluation, and methodological limitations, while answering the research questions. Chapter 7 concludes the study by summarizing the key contributions, highlighting potential applications, and outlining future research directions.

2 Literature review

2.1 Bicycle Safety Analysis

With an increasing share of cycling in everyday life as a means of transportation, driven by rising awareness of sustainability and health benefits, providing comfortable cycling environments has become an essential part of city planning worldwide. The importance of mobility planning in such a way that supports cyclists has also become a central topic in transportation research. Among different research topics aiming to promote cycling, the improvement of safety is a commonly addressed theme, as there is a high number and rate of traffic accidents involving cyclists, where they get injured or lose their lives. Research on traffic safety surrounding cyclists can be categorized into several key areas based on the methodologies employed. Data-driven analysis focuses on identifying large-scale patterns, examining accident statistics, georeferenced datasets, and spatial clustering [Morrison et al. 2019]. Behavioral analysis examines how road users interact with and perceive dangers using tools such as video observation, virtual reality experiments, and questionnaires[Useche et al. 2022]. System- and policy-oriented approaches focus on the institutional frameworks that affect cycling safety and explore regulatory aspects through policy analysis [Kahlmeier et al. 2021. The scale of the study area varies depending on the research goal of each approach. Macroscopic research examines the broad trends and spatial patterns of bicycle accidents and risks within a road network, deriving conclusions that are often used as safety indicators at the city level. On the other hand, microscopic studies identify specific accident hotspots or uncover local factors affecting the safety of cyclists at the segment level. Within this microscopic perspective, an increasingly common objective of research is to assess existing cycling infrastructure using standardized indicators of safety and quality. Such systematic frameworks consider a range of factors that contribute to a comfortable cycling experience. To raise examples of existing systematic assessment indicators, there are Bicycle Level of Service (quantitative; infrastructure-based) [Kazemzadeh et al. 2020], Copenhagenize Index (qualitative; policy- and perception-based) [Copenhagenize Design Company 2025], ADFC Fahrradklima-Test (subjective; perception-based) [Allgemeiner Deutscher Fahrrad-Club (ADFC) 2024], Bikeability Index Dresden (quantitative; infrastructure-focused) [Gehring 2018], and Munich Bikeability Index [Schmid-Querg et al. 2021].

Microscopic approaches examine segment-level details of streets, providing insights into local solutions for local problems. Li et al. (2024) discussed route-level cycling safety evaluation methodologies and classified them into Actual safety, Perceived safety, and Inferred safety. Actual safety calculates the risk of riding a bicycle based on existing data such as statistics on collisions, fatalities, and bicycle trip counts, and it produces objective output. Perceived safety evaluates the risk based on user surveys and captures the subjective and psychological aspects of safety. Inferred safety is the risk estimated by measuring factors contributing to the comfort of the cycling experience, such as the proximity to motorized vehicles, relative speeds of cars to cyclists, and the width of the cycling path. While Actual safety and perceived safety have been widely addressed, the insights gained are often case-specific to the target study area, making it difficult to generalize the findings and apply them to another study area. In particular, perceived safety research also presents some challenges, such as high sensitivity to contextual variability, which means that results or perceptions can be affected by varying settings, including time of day, traffic volume, or cultural background. In contrast to the above two, inferred safety research is suitable for conducting a systematic assessment of cycling facilities, as it is typically grounded in a standardized data format that describes road environments. There is significant potential for further research in the assessment of bicycles' safety as data availability expands with the advancement of data-collecting technologies. Particularly, advances in sensor technology and computational power now enable more complex analyses, which open up new possibilities for inferred safety research, that can yield new insights and findings. Because it is grounded in objectively measurable factors, this approach enables consistent and reproducible evaluations of cycling environments. In this regard, the growing availability of standardized 3D road models, such as CityGML, presents a promising direction for future research due to their consistent representation of geometry and semantics. A pioneering study evaluating cycling infrastructure at the segment level using CityGML was conducted by Beil et al. (2024). This study quantified geometric and semantic information regarding cycling lanes included in semantically rich CityGML data. The information extracted includes, for example, path width, slope, and parameterized proximity to local disturbances. Based on these data, a sequence of geoprocessings on FME is developed, which derives Bicycle Level of Service (BLoS) values. The process is repeated under different cycling volume scenarios to gain insights into how variations in traffic demand affect the service quality of individual path segments, to identify local bottlenecks, and to compare existing conditions with planned infrastructure improvements.

While the studies introduced above consider several parameters that influence riding comfort and safety, a critical component, visibility, remains underexplored within inferred safety analyses. As visibility has a significant impact on the likelihood of accidents and the inter-

actions between cyclists and other road users, attempts to quantify and integrate visibility into safety indices are likely to provide useful insights. Therefore, as a crucial component of evaluating bicycle infrastructure, the section that follows concentrates on road safety research related to visibility to explore the way to construct methodologies that incorporate this factor.

2.2 Visibility and Road Safety

Visibility plays a critical role in cyclists' safety, especially in urban settings where infrastructure is densely built and interactions with vehicles are frequent. Studies have shown that poor visibility is a significant contributor to traffic accidents along transportation corridors [Jung et al. 2018]. The risk is particularly high for vulnerable road users, such as bicyclists and pedestrians. According to a compilation of crash data from the US, the second-highest contributing factor of collisions involving bicycles or pedestrians was limited visibility [González-Gómez et al. 2021]. Similarly, when focusing on cyclists' fatal accidents, poor visibility conditions were identified as the second leading cause, following failure to yield the right of way and improper crossing behavior [González-Gómez et al. 2021]. The likelihood of cyclists being involved in accidents is high due to their smaller size, which can lead to them being overlooked. Furthermore, the risk of severe injury in a collision with motorized vehicles is high due to relatively lower levels of protection [Brown et al. 2021]. Despite the vulnerability of cyclists and other non-motorists, it is often the case that roads are designed to ensure comfortable and safe manoeuvres from the motorists' point of view, with little consideration given to other road users.

2.2.1 Sight Distance

The quantification of the sight availability on roads is well established in road designs for motorists and the inspection of available sight is often a subject in road safety research. It is a method often employed in highway designs because insufficient sight immediately leads to the higher risk of a serious accident. A common quantification method of sights is available sight distance (ASD) analysis [Bassani et al. 2015]. In sight distance analysis, the distance to the farthest visible point of the path ahead from an observer (road user) is compared to the distance necessary for the user moving at statutory speed to come to a complete halt safely. The former is called available sight distance (ASD), and the latter is called stopping sight distance (SSD) or required sight distance (RSD). RSD is mainly impacted by the speed of vehicles, deceleration rate, time which drivers normally require to perceive and react to objects [González-Gómez et al. 2022]. ASD failing to meet RSD means a higher risk

of collision due to inadequate reaction and stopping time. Therefore, it is important to ensure sufficient ASD in designing new roads and redesigning existing roads. There are also subcategories of sight distances according to specific maneuvers, such as overtaking a slower vehicle PSD (Passing Sight Distance), driving or turning at intersections ISD (Intersection Sight Distance).

2.3 Intersection Safety

The vulnerability of VRUs at intersections is prominent in urban areas due to the high density of the street network and the presence of various destinations, resulting in many crossings of paths used by road users of different modes [González-Gómez et al. 2022]. Although most urban streets have lanes dedicated to each transport mode, such as sidewalks, cycling lanes, and roads for respective road users, their paths often cross at intersections, making them hotspots for numerous conflicts. Visibility plays a key role in the safety at intersections. While effective traffic control systems, such as traffic signals, are vital, visibility also plays a key role, as human factors significantly affect safety when the system does not entirely resolve conflicts. Due to the high number of conflict points, road users must simultaneously scan the movements of many others, which disperses their attention and increases the risk of overlooking someone. For the above reasons, the geometric design of intersections and obstruction-free surroundings is crucial in preventing accidents caused by limited visibility. Road regulations in many countries emphasize these design principles to enhance sightlines and reduce blind spots for all road users, as introduced in section 2.2. Intersection-specific visibility design principles are often defined in terms of intersection sight distance (ISD) and sight triangle in road design regulations in many countries. The following section focuses on these design principles and looks into concrete design speculations in Germany.

2.3.1 Visibility-based Design Principles at Intersections

Intersection Sight Distance (ISD) and the sight triangle are fundamental components in intersection design, ensuring safe and efficient vehicle movements. ISD represents the minimum distance along the crossing road that a driver must be able to clearly see to decide whether it is safe to proceed, especially when they do not have the right of way, such as in the presence of a stop or yield sign [González-Gómez and Castro 2019]. The sight triangle, on the other hand, is an area connecting three nodes: the observer point, the target point on the conflicting path, and the conflict point. Legs bound it along two roads and the driver's line of sight. It is located at a corner of an intersection, and the area inside the triangle should be free of visibility obstructions to provide sufficient visibility for both approaching road users.

Two sight triangles will be formed if a road user needs to traverse a two-way intersection, as they must pay attention to vehicles approaching from both the left and right as shown in Figure 2.1. In urban areas, where intersections tend to be more congested and the risk of conflicts is higher, it is particularly critical to maintain the sight triangle free of obstructions [Kilani et al. 2021]. The concrete dimensions of sight triangles vary depending on countries,

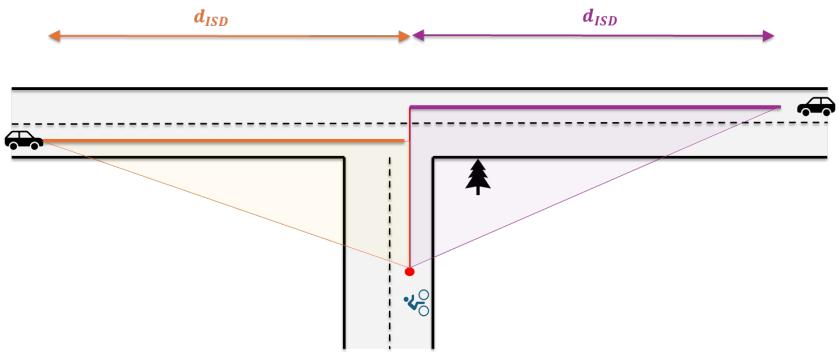

Figure 2.1: Sight triangles at an intersection with two-way major road

and they are often differentiated according to the intersection types and design criteria, which include the kind of traffic control present (signals, stop, yield signs, or roundabout), and whether the control is applied to a significant or minor approach [González-Gómez and Castro 2019]. Sight triangles at uncontrolled or unsignalized intersections are crucial. Their sight triangles consist of a short leg and a long leg, with one vertex placed on a minor road at a stopping line and the other vertex placed at a point on a major (priority) road at a distance equal to the stopping distance from the conflict point (Figure 2.2). The length of this

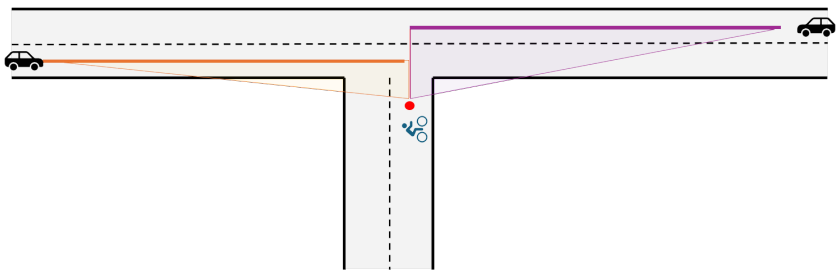

Figure 2.2: Sight triangles at an unsignalized intersection with two-way major road

long leg is determined by various factors, typically including the speed of the major road, friction, and slope, but it is primarily based on the design speed of the major road. To ensure safety, the formulas used to calculate this distance in many places are generally conservative, meaning they tend to assume slightly longer distances than would be necessary in practice. The values speculated in German road designs will be introduced in the following section.

2.3.2 Intersection Sight Distance in Germany

In Germany, several official guidelines address road design and sight distance at intersections [StVO2Go 2022]. Keys among these are

- **RASt 06** – Guidelines for the Design of Urban Roads (*Richtlinien für die Anlage von Stadtstraßen*) [Forschungsgesellschaft für Straßen- und Verkehrswesen (FGSV) 2006]
- **R-FGÜ** – Guidelines for the Design and Equipment of Pedestrian Crossings (*Richtlinien für die Anlage und Ausstattung von Fußgängerüberwegen*) [Forschungsgesellschaft für Straßen- und Verkehrswesen (FGSV) 2001]
- **RAL 2012** – Guidelines for the Design of Rural Roads (*Richtlinien für die Anlage von Landstraßen*) [Forschungsgesellschaft für Straßen- und Verkehrswesen (FGSV) 2012]
- **RAA** – Guidelines for the Design of Motorways (*Richtlinien für die Anlage von Autobahnen*) [Forschungsgesellschaft für Straßen- und Verkehrswesen (FGSV), Working Group Highway Design 2008]

All these guidelines highlight the importance of sight triangles at intersections for drivers, cyclists, and pedestrians to secure mutual visibility. Among these design standards, RASt explicitly addresses requirements for intersection sight distance involving cyclists in urban environments and explains the dimensions of sight triangles that should be clear of visual obstructions. RASt specifies the sight triangles depending on intersection control (signalized, unsignalized priority, stop, or yield control), but the most determinant factor is whether a cyclist has right-of-way. Another factor considered in RASt is whether a cyclist travels on-road (in mixed traffic) or off-road (on a dedicated cycle track crossing the intersection), as the visibility of cyclists is better when their path is mixed with motorized traffic than in a separated cycle track. The guideline assumes that road users without RoW respect the priority rules, drive safely, and thus stop or yield when they must do so.

The sight triangle dimensions are simply summarized as follows.

- When a cyclist is at a signalized intersection, there is no need for a sight triangle, as the traffic signal resolves the conflict
- When cyclists are on a priority road at an unsignalized intersection (conflicting paths have to stop or yield), cyclists need to be seen by vehicles entering the intersection. Cycling lanes extending up to 30m upstream of conflict points should be visible, considering the speed and direction of cyclists. In a complex urban environment, the length of this long leg of the triangle can be 20m. The vehicle driver's decision point is at the stopping line, which is 3m from the edge of the intersection, as per the design guidelines, unless a stop line is present.

- When a cyclist is on the minor road at an unsignalized intersection (conflicting paths have RoW), cyclists need to stop or slow down and have a clear view of crossing traffic as far as the ISD for motorists on the major road, which corresponds to the long leg length. The distance is primarily determined by the design speed of the major road, as shown in Table 2.1 below [Magyari and Koren 2018]. The decision points for cyclists are the same as those for vehicles if otherwise specified by road markings. It has to be noted that these ISD figures are taken from ISD for two vehicles approaching an intersection as ISD specifically for cyclists is not available.

Table 2.1: Design speed and intersection sight distance

Design speed of major road	ISD
30 km/h	30 m
40 km/h	50 m
50 km/h	70 m

In addition to the horizontal dimensions, RASt mentions the vertical sight field, which should be maintained free of obstruction (0.8 m to 2.5 m above ground) and can be caused by parked vehicles or vegetation. The sight blockage is significantly influenced by the height of objects and the eye height of road users [Jung et al. 2018]. RASt [Forschungsgesellschaft für Straßen- und Verkehrswesen (FGSV) 2006] assumes the following height of the eyes for each.

Table 2.2: Road users' defined eye height

Observer	Eye height
Car Driver	1.0-1.2 m
Lorry Driver	∼2.0 m
Cyclist	∼1.5 m

To ensure that cyclists can detect other road users and minimize the likelihood of collisions, cycling facilities must be designed with adequate sight distances [González-Gómez et al. 2021]. In reality, securing a clear vision through sight triangles with the recommended size in the guidelines is not always possible in densely built-up urban environments [Kilani et al. 2021]. If the sight distance shortage is evident during the design phase, mitigating measures through location-specific traffic control should be taken. However, the available sight distance is not static, as landscapes change over time due to the growth of vegetation or the installation of new roadside features. Therefore, regular inspections of sight distance should be conducted to ensure that the current conditions remain safe and the intersection's design and control measures remain effective.

2.3.3 Frequent accident types at intersections in Germany

Intersections account for the majority of bicycle–motor vehicle crashes in German cities [Schröter et al. 2023]. Accident statistics show that about two-thirds of cyclist injury accidents involving another road user occur at junctions, intersections, or driveways [Statistisches Bundesamt (Destatis) 2022; Unfallforschung der Versicherer (UDV) 2013]. The accident situations that represent the most frequent and characteristic patterns are right-hook collisions, left-turn collisions, near-side crossing collisions, and far-side crossing collisions as illustrated in Figure 2.3.

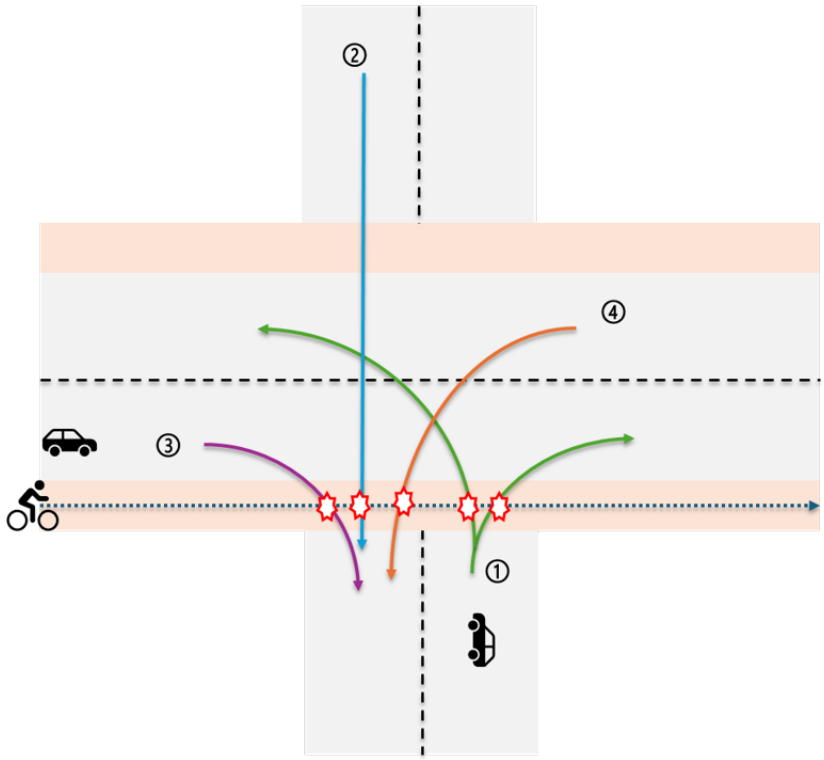

Figure 2.3: Common accident types and conflict points

1. Near-side crossing collision happens when a vehicle exits a minor street or driveway and collides with a cyclist coming from the left on the priority road. This pattern is strongly affected by visibility obstructions such as parked cars, vegetation, or building corners that block the line of sight between the motorist and the cyclist [Unfallforschung der Versicherer (UDV) 2013]. According to empirical research, accident risk increases when cycle tracks are placed several meters away from the main vehicle path, because drivers fail to look far enough to the left to detect cyclists in time [Allgemeiner Deutscher Fahrrad-Club (ADFC) e.V. 2020; Unfallforschung der Versicherer

(UDV) 2013].

2. Far-side crossing collision occurs when a motorist crosses an intersection from a side street collides with a cyclist approaching from the right side on the main road after crossing vehicle paths. This type of accident is less frequent than near-side cases. It is often associated with wrong-way cycling, where cyclists ride against the lawful direction of movement [Unfallforschung der Versicherer (UDV) 2013]. This leads to drivers not expecting any cyclists approaching them, and recognition is delayed. The collisions often happen at higher speeds, leading to severe injury outcomes [Gesamtverband der Deutschen Versicherungswirtschaft e.V. (GDV), Unfallforschung der Versicherer (UDV) 2025; Statistisches Bundesamt (Destatis) 2022].

3. Right-hook occurs at a situation where a motorist turns right while a cyclist continues straight ahead on the same street. This is one of the most frequent and severe types of urban bicycle accidents. Statistics indicate that around one in five intersection accidents involving cyclists result from a right-turning vehicle cutting across the cyclist's path, with trucks presenting the highest fatal risk due to their larger blind spots [Unfallforschung der Versicherer (UDV) 2013]. In more than 90% of cases, the main cause of this accident pattern is driver's error, especially failure to yield or omission of the required shoulder check [Gesamtverband der Deutschen Versicherungswirtschaft e.V. (GDV), Unfallforschung der Versicherer (UDV) 2025]. Situations that can cause this type of collision include simultaneous green light arrivals and high cycling speeds [Buch and Jensen 2017].

4. Left-turn hook occurs when a motorist turning left across opposing traffic collides with a cyclist riding straight from the opposite direction. Such collisions are common at signalized intersections, where both movements are often permitted simultaneously [Wang and Nihan 2004]. Accident analyses indicate that these conflicts primarily arise from misjudging the cyclist's speed or failing to notice the approaching bike altogether [Unfallforschung der Versicherer (UDV) 2013]. The responsibility lies almost exclusively with the motorist, as German traffic law grants priority to oncoming traffic, including cyclists.

2.4 3D Road Visibility Analysis Case Studies

As the state of the roads at an intersection can change over time, available sight can also be drastically affected in some cases. The assessment of sight distance on existing roads is conducted through direct field measurements or indirect digital measurements [Bassani

et al. 2015]. The first case requires the partial or complete closure of the target road during the survey time, which exposes the field survey operators to ongoing traffic and thus creates a risky working environment [Bassani et al. 2015, Kilani et al. 2021]. Due to the nature of manual work, the extent of data that can be collected is limited, and the amount of time and effort necessary to obtain adequate data for applications is significant. The second case is becoming increasingly common in the transport research field, mainly due to the advancement of remote sensing technologies that enable to capture road geometry, making digital data-driven analysis possible. The growth of computational capabilities in today's computers also contributed to allowing the processing of complex 3D geospatial data. The applications of realistic 3D geospatial models and data have made significant progress in road visibility research over the past few years. There has been an increase in research using point cloud data, combined with digital surface models (DSMs), to quantitatively assess visibility. These data also allow for the simulation of road users' views in a realistic manner across various traffic conditions. This digital approach offers greater flexibility in creating simulation environments and provides new insights into how environmental and infrastructure factors affect visibility.

2.4.1 Case Studies

Kilani et al. (2021)] developed an automated framework that utilizes mobile LiDAR data to map and detect obstacles that can have a negative impact on the visibility of drivers approaching intersections in an urban setting in Edmond, Canada. The evaluation was conducted based on blockage percentage, which was calculated as the proportion of sightlines within the intersection sight triangle blocked by surrounding objects. The evaluated values are then statistically compared with historical collisions in order to reinforce the relationship between poor visibility and collision risks. The entire procedure, from data input of LiDAR point clouds to blockage percentage output, was programmed in MATLAB to minimize the need for manual intervention.

Bassani et al. (2015) presented a comprehensive analysis methodology for ASD using LiDAR-based Digital Surface Models (DSMs) and ArcGIS software. The study investigated a transportation corridor with a high number of potential visibility obstructions densely built along in Turin, Italy. The data was collected using a mobile mapping device, and a detailed 3D representation was built on GIS as DSM data. A customized sequence of geoprocessing procedures for visibility analysis was made using the built-in ModelBuilder algorithm to realize automation. The analysis identified the roadside elements contributing to critical reductions in available sight distance and recommended interventions, such as removing parking lanes to secure sufficient visible distance.

In another approach by González-Gómez and Castro (2019), 3D visibility analysis was performed at urban intersections in Madrid, Spain, to investigate the effects of roadside elements on the available sights for cyclists and other VRUs. The analysis collected 3D data on the target location with LiDAR technology and analyzed GIS software using the LoS geoprocessing tool. The authors systematically evaluate the ASD of the subject VRUs at regular intervals along their paths across. Their method was tested at multiple intersections with different geometrical configurations. Changing ASDs corresponding to the position of cyclists approaching a T-junction and a roundabout were determined, and the values were compared to standard SSDs. The results show that the presence of street furniture and vegetation significantly hinders the visibility for cyclists.

In a later study, González-Gómez et al. (2021) focused on vulnerable road users (VRUs), including cyclists and e-scooter riders, to investigate their conflicts at two urban intersections in Madrid. The first analysis compared ASD with SSD for cyclists and e-scooter riders under different vegetation conditions (actual vs. modified with 3D assets of shrubs) to assess their influence on sight distances. The second analysis involved an intervisibility analysis through a sight triangle between VRUs, with two scenarios differing in vehicle traffic conditions (absence vs. presence of parked and queued vehicles). The study demonstrated how specific design changes could improve mutual visibility.

In their recent work, González-Gómez et al. (2022) extended their methodology by introducing scenario-based analysis to differentiate and quantify the effects of roadside elements on drivers' visibility toward VRUs, according to the types and position of the obstructions. Various configurations of parked vehicles, vegetation, and street furniture were introduced as modified versions and enhancements and are compared to the raw captured data. The findings highlighted that large vehicles, such as vans parked near pedestrian crossings, and significant urban elements, including trash containers, severely hindered drivers' views of VRUs. The modified scenarios demonstrated that removing or repositioning these obstructions is effective in enhancing visibility.

Jung et al. (2018) conducted a viewshed analysis at a four-leg intersection in Oregon, USA, incorporating diverse observer parameters to reflect multi-modal usage of the intersection. The target road users included heavy vehicles, passenger cars, cyclists, and pedestrians, and their points of view were reconstructed by elevating them to their respective eye heights and positions. Additionally, the authors incorporated a dynamic element into the analysis, particularly by investigating the changing perspective within the turning movement. The study revealed that a slight change in observer height has a significant impact on visibility, with observers at lower eye heights experiencing more frequent and severe blockages.

2.4.2 Methodological Limitations in Existing Studies

Although the recent case studies described above collectively demonstrate the growing development of 3D data and GIS-based methodologies, certain limitations remain in their approaches. A key concern is the mostly motorist-centric perspective of existing research. VRUs' perspectives have not been fully explored despite the eye height differences, different speeds of movement and having often dedicated lanes separated from driving paths. In addition, generally, the intervisibility between different types of road users is rarely addressed.

Cyclist-centered road safety research itself related to their visibility exist but the methodological focus of current research is on perceived safety, which encompasses human psychological perception factors, such as the rider's reaction to specific traffic situations. The lack of geospatial data-driven research may be attributable to the narrow cross-sections of the space used by VRUs, which do not allow vehicle-mounted mobile mapping systems to record the surroundings [González-Gómez et al. 2021]. Moreover, the existence of dense vegetation or city furniture along the paths blocks the laser beams or camera vision, resulting in incomplete data collection.

Additionally, existing studies focus on specific target streets or intersections, and the extendibility or generalizability of the applied methodology has not been the main topic of discussion, which can limit the insights gained through these studies to the local environment.

Lastly, when it comes to ASD studies, although the available distance is often summarized in a graph to compare with SSD or ISD to reveal the points where ASD drops under these criteria, the identification of the reason contributing to the decrease of ASD is not always discussed. Even when it is, the generalization or patterns of each visibility-blocking object have not been established, and therefore, the current findings are helpful in a limited context only.

2.4.3 Technical Limitations in Existing Studies

As mentioned in the studies introduced above, LiDAR is widely employed in road visibility studies today. However, this technology, despite its ability to capture high-quality environments, has specific challenges to overcome in order to extend its applicability. The first is the processing demand that the raw data requires. As the collected point cloud data contains noise, it is often necessary to preprocess it significantly to convert to another representation format or filter out inaccuracies before using it as input in a sight analysis software platform [Jung et al. 2018]. The data generated by LiDAR is not inherently interoperable, as it consists of unstructured points. Interpreting clusters of points as meaningful objects requires a substantial amount of work, including time-consuming and resource-intensive identification

and labeling processes. In the context of sight analysis research, some studies, such as by Kilani et al. (2021), address this challenge with voxelization techniques to examine whether voxels, which represent the space as volumetric grids encompassing the dots, intersect sightlines between on-road targets and observers. Others employ machine learning approaches to automate the recognition and categorization of road features in the point cloud data [Gargoum and Karsten 2021]. Despite the purely geometric nature of LiDAR data, standardized methods for enriching the data with semantic information are not established. As a result, the style and the extent to which the data are semantically enhanced are determined by the specific research interest. In the absence of semantic information, it is challenging to distinguish between permanent static objects, such as road geometry and buildings, from temporary static objects that happened to be in the scene when mobile mapping took place. Without classifications, it is difficult to define the base state of the road environment that excludes transient elements. The reliability of the digitally generated scene as a testbed for visibility analysis is, therefore, limited.

Given these limitations, the use of semantic 3D city models, such as CityGML, as input for 3D scene building has been gaining attention [Bassani et al. 2015]. The following section introduces 3D data models that not only support the whole 3D geometry but also enable the attribution and classification of urban features, which are key capabilities for advanced visibility analysis.

2.5 CityGML

In contrast to the widespread use of point cloud data and DSM/DTM-based methods, as well as LiDAR-based methods, in road visibility studies, the application of semantic 3D city models, particularly CityGML, remains scarce. However, these models offer distinct advantages that make them highly suitable for advanced visibility analyses in urban environments. CityGML enables the structured representation of urban features, not only in terms of detailed 3D geometry but also through rich semantic classification and object hierarchies [PLATEAU Project, Ministry of Land, Infrastructure, Transport and Tourism (MLIT) 2025]. Features such as buildings, trees, traffic infrastructure, and road surfaces can be individually defined, attributed, and related across multiple Levels of Detail (LoDs), allowing for flexible scaling of analysis and precision.

This semantic depth supports a range of visibility use cases that exceed what purely geometric or raster-based formats can achieve. For instance, specific classes of objects, such as vegetation or road signs, can be isolated or modified to simulate design alternatives. Additionally, the topological consistency and interoperability of CityGML make it well-suited for integration with traffic simulations, urban planning tools, and GIS-based evaluations. With

its capabilities, CityGML can overcome the limitations present in prior visibility studies, which tend to favor point-based or surface-based approaches. The present work, therefore, contributes a novel perspective by applying a CityGML-based framework to visibility assessment, demonstrating its potential to support more nuanced, scalable, and context-aware analyses in complex urban settings. Its design enables the derivation of models from various data sources for multiple applications, making it a comprehensive framework for intelligent urban modeling [Beil et al. 2020].

2.5.1 Definition

OGC City Geography Markup Language (CityGML) is an open conceptual model standard that establishes a common semantic information model for 3D urban objects, enabling their use in various applications. The Open Geospatial Consortium (OGC) is responsible for maintaining it as a global standard for characterizing the geometry and semantics of topographic objects in three-dimensional contexts [Labetski et al. 2018]. The first version (v1.0) of this 3D model format was first developed in 2008, and since then, the version has been updated to 3.0 today [Tan et al. 2023]. CityGML distinguishes itself from other 3D formats, such as polygon meshes and point clouds, by providing a semantically rich and interoperable framework.

2.5.2 Structure and Format

As introduced above, CityGML is a standard that defines both a conceptual model and an encoding specification for storing and exchanging 3D city models. The conceptual model specifies the features that should be included in a 3D city model, their attributes, and the relationships between features [Kurokawa 2023]. This model is described using UML class diagrams. The encoding specification defines how to encode data based on the conceptual model. CityGML adopts the Geography Markup Language (GML), an XML-based language specialized for geospatial information, and specifies an XML Schema for encoding 3D city models in GML [Kurokawa 2023]. The XML Schema defines the XML tags corresponding to features, attributes, and relationships in the conceptual model, as well as the order and number of occurrences of these tags. Data created in accordance with this XML Schema constitute the 3D city model data [Kurokawa 2023]. CityGML enables extensibility through Application Domain Extensions (ADEs), allowing users to add custom concepts, classes, or attributes to the data model. These extensions are defined using XML Schema Definition (XSD) files, similar to the core CityGML model. ADEs can be created using either XSD or UML, allowing for the tailoring of the model to specific domain needs [Schwab et al. 2020].

CityGML comprises four levels of detail (LoD), ranging from 0 to 3, where the geometric

and semantic complexity of the model increases, thereby approximating real-world objects more realistically [Biljecki et al. 2015]. This concept is applied not only to the geometric aspects of objects, but also to their semantic aspects. The differences between Levels of Detail (LoDs) vary depending on the module. For example, in the geometric representation of building exteriors, LoD0 depicts simple building footprints, LoD1 represents buildings as block-shaped cuboids, LoD2 includes detailed roof shapes, and LoD3 models the whole exterior, including roofs, doors, and windows. Higher LoDs are not always available, as they require more accuracy-dependent data collection. The appropriate LoD for a given application should be selected based on the specific requirements and objectives of that application. For instance, a simulation might need complete building shapes for a building-level energy assessment, but a navigation system might need basic road lines. LoDs facilitate the matching of data to its intended use [Biljecki et al. 2015].

CityGML comprises a core module at its base, which describes common properties applicable to all objects, as well as thematic modules built upon it, such as Building, WaterBody, and Transportation. The module composition of the latest version of CityGML is shown in Figure 2.4. The CityGML core (green) defines basic concepts and spatial attributes that are inherited by all other modules. Modules in blue in the figure define concepts applicable to all thematic modules, which contain different city objects individually, expressed in red.

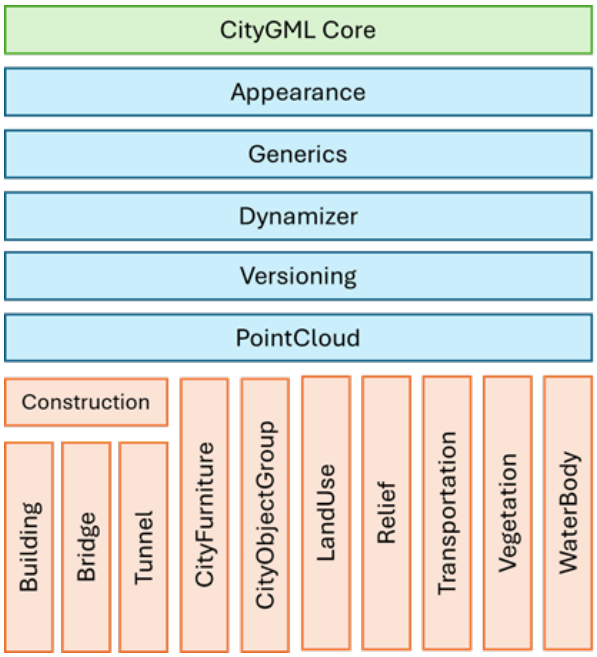

Figure 2.4: CityGML modules [Kutzner et al. 2020]

2.5.3 Version 3.0 and lane model

Since its establishment, CityGML has undergone updates, and the latest version, CityGML v3.0, is currently available. V3.0 now includes new modules, such as Dunamizer, Versioning, PointCloud, and Construction, while existing modules, including Core, Generics, Building, and Transportation, have been revised. Among these changes, the transport module saw significant improvements through the update to v3.0, as data models for road infrastructure, including roads, pedestrian pathways, and railways, were enhanced. Individual lanes are now available as distinct objects [Kutzner et al. 2020]. This opens up the possibility for applications, as semantic information attached to each distinguished object becomes usable, and a hierarchy among objects can be defined. The transportation module has the following hierarchical structure.

In the Transportation module, Roads, Railways, Tracks, and Waterways define the highest-level networks. Sections and Intersections are their subdivisions, categorized according to whether they represent continuous stretches or crossing points. TrafficSpaces and AuxiliaryTrafficSpaces are rooms designed for traffic movements, and TrafficAreas and AuxiliaryTrafficAreas are the ground areas at the bottom of these spaces, respectively [Technical University of Munich (TUM), Chair of Geoinformatics 2023]. In the LoD3 of the transportation module, individual traffic lanes are available under Traffic Area and Traffic Space [Beil et al. 2020].

3 Data and Methodology

The methodological framework is designed to incorporate materials and tools that address the limitations identified in the current visibility studies, such as a motor-centric approach, a static nature, and a lack of semantic information about urban objects. This thesis aims to address the recurring research gaps found in the literature and to develop systematic and reproducible methods for quantifying visibility, which have been rarely explored, as most studies focus on specific intersections or road segments. Given these research gaps, the thesis proposes a framework that leverages novel semantic 3D city models (CityGML v3.0) in combination with parking data from TIAS to systematically assess cyclist visibility at intersections. It is done by quantifying the impact of various urban road elements on the reciprocal visibility of cyclists and vehicle drivers. While tackling the visibility analyses, the usefulness of the two novel datasets included in this analysis, CityGML and TIAS, will be assessed. Furthermore, the methodology adopted in this study is designed to automate procedures, thereby achieving scalability and reproducibility, rather than limiting the analysis to a single case study. It develops transferable procedures that can be applied to multiple intersections and extended across urban networks. This systematic methodology contributes to addressing the lack of generalized, data-driven, and semantically informed visibility analyses in current literature.

This chapter first outlines the required datasets and their acquisition sources for constructing realistic traffic scenes, along with their specifications. It then introduces multi-layered scenarios, each designed to assess the impact of specific urban elements on cyclists' visibility. Following this, analytical approaches for different accident types are presented, after which the concrete analytical tools and their detailed workflows are described. Finally, the processes for quantifying each type of analysis and identifying visibility-blocking elements are described.

3.1 Data Acquisition and Requirements

The first step of this study involves collecting the necessary data to replicate a 3D scene within the ArcGIS Pro platform. The analytical framework is based on three complementary data sources, representing different classes of urban elements: permanent static features,

temporarily static objects, and roads themselves.

- Driving and cycling path: Lane Model (CityGML)
- Permanently static components: Buildings, City furniture, and Vegetation (CityGML)
- Temporarily static components: Virtual parked vehicles derived from TIAS segmentation results

The detailed data acquisition methods, requirements, and specifications for each data type are described below.

3.2 CityGML Datasets

CityGML provides the semantic and geometric foundation of the analysis. The transportation module in CityGML v3.0 offers a lane-level road model, where driving lanes, bicycle paths, sidewalks, and parking areas are distinguished under layers such as TrafficArea and TrafficSpace. The centerline of each lane within TrafficArea can be included in the dataset as TrafficSpace_line, representing the path of cyclists and drivers, assuming that the viewpoints of these road users lie on the centerline of their respective lanes. Each feature has its own unique GML ID and semantic information, including a dedicated road usage type (driving, cycling, parking, or tram) and a designated speed limit, which is available as part of the attributes. A TrafficSpace is assigned to one specific function, which means that overlapping or shared areas, such as intersections or mixed-use zones, are not represented by single features but rather as individual TrafficSpace features that geometrically overlap.

CityGML transport module used in this study is derived from ASAM OpenDRIVE, an open, XML-based, industry-standard format for the detailed and logical description of static road networks, which includes lane geometries, junctions, and road markings [Association for Standardisation of Automation and Measuring Systems (ASAM) 2025]. This data standard is free to use and is widely applied in the automotive and transport fields for testing, simulation, and the development of automated driving systems. OpenDRIVE datasets can be created using road design software or converted from existing digital maps. Simplified versions can also be made from OpenStreetMap, though only for drivable roads. Detailed datasets can be produced from accurate geospatial data, such as LiDAR scans or photogrammetric surveys.

A fully compliant CityGML dataset for roads can be generated from OpenDrive datasets using the road-space converter r:trån, developed by the Chair of Geoinformatics at TUM, which enables seamless integration within GIS ecosystems [Technical University of Munich (TUM), Chair of Geoinformatics 2025]. The dedicated direction of the movement on each

lane, the usage, and design speed included in the original OpenDrive dataset can be transferred as semantic data in the generated CityGML datasets. The CityGML transport datasets used in this study are obtained from the TUMDOT-MUC (Trajectories from Urban Multimodal Drone Observations of Traffic – Munich) project by the Chair of Traffic Engineering and Control at TUM, and from the tum2twin project led by an interdisciplinary team from TUM [Technical University of Munich (TUM), Chair of Traffic Engineering and Control 2025, Technical University of Munich (TUM) 2025]. The former was a project aimed at creating a comprehensive dataset for studying traffic and mobility, covering the area along Rheinstraße in the Schwabing district of Munich. The latter was a research initiative aimed at creating a large-scale, open-source dataset for Munich's urban digital twin. The project's focus is on the area surrounding TUM in the downtown Maxvorstadt district. These study locations with available CityGML transport datasets are described in Figure 3.1.

Rheinstraße is an urban road section stretching about 700 m between Bonner Platz and Leopoldstraeße. This road section represents a typical inner-city two-way arterial intersected by a few mixed-use streets and two major streets at the ends. Designated bike lanes are primarily present along Rheinstraße, separated from driveways and pedestrian sidewalks. The surrounding area comprises residential buildings, a school, a sport facility, and public transport stops such as Bonner Platz and Potsdamer Straße. The CityGML transport datasets for this study area was obtained as OpenDRIVE dataset made available at the project's website [Technical University of Munich (TUM), Chair of Traffic Engineering and Control 2025]. It was created for this project using drone imagery, existing geospatial data, and manual annotation.

The second study area covers a section of the Maxvorstadt district centered around the main campus of the Technical University of Munich The area is characterized by a dense lattice-like street pattern with perpendicular intersections, a mix of primary, secondary and residential roads, as well as the presence of one-way streets, tram lines. It also includes courtyards and open spaces belonging to museums, university facilities, and cultural institutions. The area features high pedestrian activity associated with university buildings cultural facilities. Traffic lane data for this study area was obtained from tum2twin's project webpage. The original data was modeled based on high-resolution orthophotos in Mathworks RoadRunner, where HD (high-definition) map was manually constructed. The HD map was exported as an OpenDRIVE dataset, which forms a detailed digital representation of the transport infrastructure in this study area [Wysocki et al. 2025].

For both study sites, additionally, city furniture, vegetation, and building layers are added to the scene from CityGML datasets to represent permanently static roadside objects. City furniture was captured during the data collection campaign within TUMDOT and the tum2twin project using laser scanning technologies along with the road data capturing. The geome-

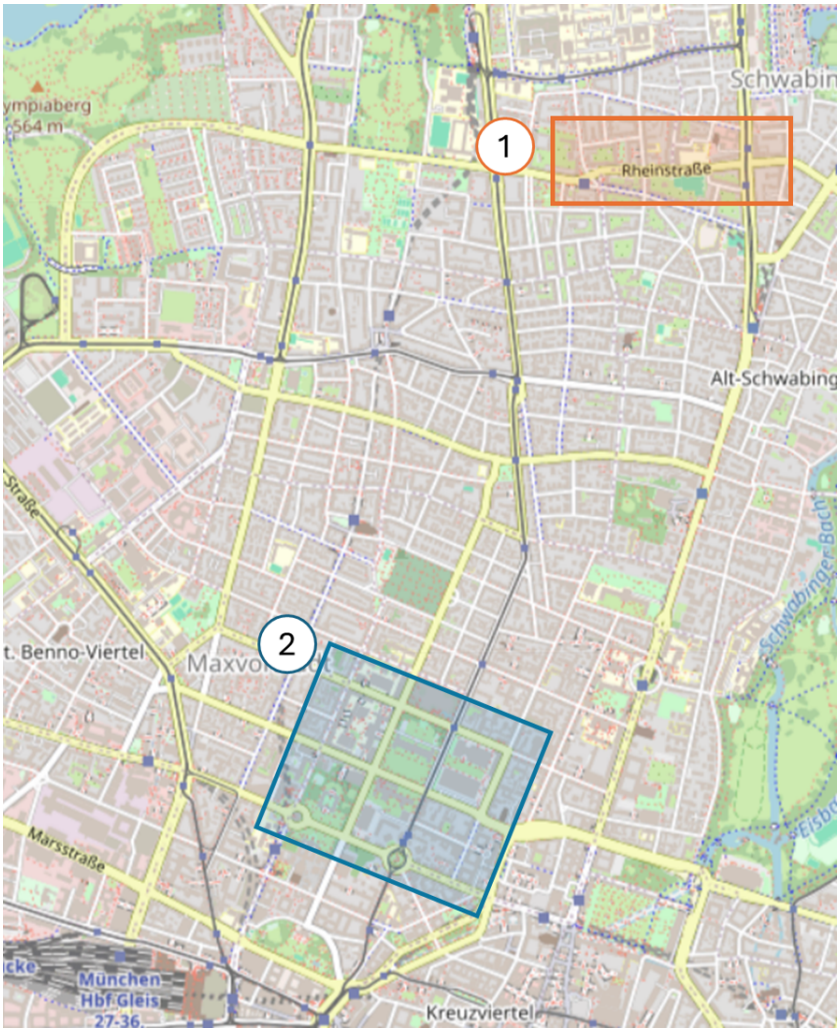

Figure 3.1: Two study areas. Orange area is Rheinstraße and blue area is the area around TUM

try of this layer is either the original shape digitally preserved as 3D objects or replaced by simple 3D assets. Vegetation data is obtained from Solitary vegetation models, in which vegetation objects for the entire city were reconstructed using aerial imagery and ALS point clouds in a study led by Münzinger et al. (2022). 3D models of trees are reconstructed by using geometric primitives to approximate the shape of the tree crowns. As for building data, TUMDOT opendrive dataset obtained through the projects' webpage already included buildings, which could be converted into CityGML building layer in LoD2, while the study area near TUM did not directly provide building data within its opendrive datasets, so the 3D building models corresponding to this study area was obtained from Bavarian State Office for Digitizing, Broadband and Survey (LDBV) [Bayerische Vermessungsverwaltung

2025]. The source of datasets are summarized in Table 3.1.

Table 3.1: Data Sources by Area

Area	Data	Source / Project
Rheinstraße	City Furniture	TUMDOT
Rheinstraße	Vegetation	Solitary vegetation models
Rheinstraße	Buildings	TUMDOT
Rheinstraße	Lane Model	TUMDOT
Area around TUM	City Furniture	tum2twin
Area around TUM	Vegetation	Solitary vegetation models
Area around TUM	Buildings	3D-Gebäudemodelle Bayern
Area around TUM	Lane Model	tum2twin

3.3 TIAS segmentation result dataset

The data generated through a model trained on Traffic Infrastructure and Surroundings (TIAS) dataset enriches the 3D traffic scene with parking-related information. The literature review identified parked vehicles as a key, yet underrepresented, obstruction type in 3D visibility studies. For instance, González-Gómez et al. (2022) demonstrated that parked vans and other vehicles can severely compromise cyclist visibility, yet most earlier approaches did not systematically model parking. TIAS segmetation results supplement the 3D city data by enabling the distinction between roadside spaces designated as parking-permitted areas and non-parking-permitted areas. TIAS is developed by DLR (German Aerospace Center) in an effort to overcome critical data gaps in nationwide parking inventories by leveraging aerial imagery and integrating cadastral data, providing a comprehensive basis for urban mobility analysis and traffic safety applications [Rauch et al. 2025]. TIAS is a set of aerial images of roads with high-quality annotations indicating the type of traffic activities that occur in traffic scenes within the images. There are nine categories used in the labels, namely, (1) parking areas, (2) roads, (3) access ways, (4) blocking area (keep-out area), (5) road shoulder, (6) footway, (7) railroad bed, (8) cycle path, and (9) water. TIAS defines not only the primary use of each area but also the secondary use, accommodating the multi-functional nature of the space. Therefore, an area can be captured as a "road" for its primary use and a "parking area" for its secondary use, reflecting the roadside usage often seen in German residential areas. A limited number of city districts in Munich have manually annotated TIAS data. However, a segmentation model has been developed to automatically evaluate all the parking spaces and is used to generate parking information data for the study area of this thesis. As the TIAS-derived dataset is derived from aerial imagery, the extraction of parking usage is inevitably influenced by the specific moment of image acquisition. While

permanent parking areas, typically delineated by painted lines, are consistently classified as parking spaces, roadside parking in residential areas is only captured if vehicles are present at the time of data collection. A key strength of TIAS lies in the introduction of the "shared with parking" attribute, which explicitly accounts for the informal occupation of road space by parked vehicles. This feature is particularly relevant for visibility and obstruction studies, as it more accurately reflects the multifaceted reality of urban streets. Beyond its detailed annotation scheme, TIAS enables the creation of a more comprehensive parking inventory by distinguishing between publicly accessible, semi-private, and private parking areas. As demonstrated by Rauch et al. (2025), the Berlin case study revealed that publicly accessible parking constitutes about 60% of the total supply, highlighting the degree to which conventional datasets underestimate actual total capacity. This improved completeness is particularly important for analyzing cyclist visibility in mixed-use urban environments, where obstructions from parked vehicles can significantly impact safety. The data provided by DLR for this thesis is the extraction of areas classified as either primary parking spaces or secondary spaces by the automatic segmentation model. The data is provided in GeoJSON format as a polygon layer, as shown in Figure 3.2.

Figure 3.2: TIAS parking area extraction highlighted in green.

3.4 Scenarios and Scene Modeling

To systematically evaluate the contribution of different obstruction classes, the methodological framework adopts multi-level traffic scenarios. Similar approaches have been suggested in recent cyclist visibility research to investigate the visibility-blocking effects of different roadside elements [González-Gómez et al. 2022]. However, they often remain limited to a narrow set of obstructions. In this thesis, two primary settings are designed to identify the visibility-reducing factors in a step-by-step manner.

- **Scenario 1 (Static environment):** includes only permanent features such as buildings, vegetation, and city furniture, separately or together. It is a base scenario upon which the following scenarios are constructed.
- **Scenario 2 (With parked vehicles):** leverages roadside parking area data classified by TIAS. This addresses the influence of roadside parking on visibility, emphasized in recent cyclist-focused studies.

The scenarios and their data input are summarized in Figure 3.3.

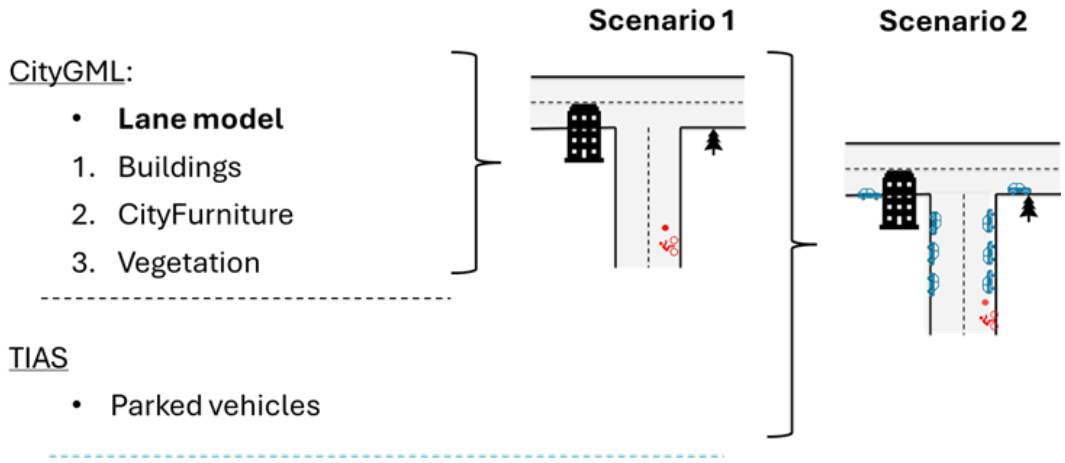

Figure 3.3: Visibility analysis scenarios

Scenario 1 focuses on static objects that function as potential sight obstructions, including buildings, city furniture, and vegetation. The effects of these elements on visibility are first examined individually to determine the degree to which each category contributes to visual obstruction within the urban environment. Subsequently, these static elements are combined within a single scene to evaluate their cumulative impact on overall visibility. In Scenario 2, the analysis is extended by incorporating parked vehicles derived from the TIAS segmentation model into the 3D environment, in addition to the static objects from

Scenario 1. This setup provides a more realistic representation of urban road usage, enabling a comprehensive assessment of visibility under typical traffic and environmental conditions.

3.5 Analytical Approaches for Accident Types

The methodological framework connects visibility analyses with accident typologies to fully capture potential causes of visibility obstructions and to derive accident-type-specific collision risk indicators linked to each intersection entry. The types of accidents considered are introduced in the literature review. To address different forms of bike–motorist collisions appropriately, the visibility analysis is structured into two parts.

3.5.1 Intervisibility Analysis During Turning Movements

The first analysis is intervisibility analysis, which evaluates whether drivers and cyclists can mutually detect each other before reaching a conflict point when a vehicle intends to make a turning movement. The collision types, "right-hook" and "left-hook", are dealt with using this analytical approach. Right-hook collisions occur when a vehicle and a cyclist move on the same street in the same direction, parallel to each other, and a vehicle turns right across a through cyclist's path. In contrast, the left-turn collisions occur when a car turns left into the path of an oncoming cyclist. This accident can occur even at signal-controlled intersections, as the cyclist and driver often receive simultaneous green signals [Saeidi Razavi and Furth 2021; Warner et al. 2017].

In contrast, the left-hook accidents occur between cyclists and motorists on the same street but moving in opposite directions. Similar to the right-hook accident, this type of collision can occur at signalized intersections when the signal is designed to allow these two trajectories to have simultaneous green lights. Cumming (2012) notes that drivers turning left at intersections primarily focus on the oncoming vehicle traffic stream in order to find a gap, while giving considerably less attention to the road users in the secondary position, where oncoming cyclists move, whose paths they must also cross. Considering the attention reduction factor, it is even more crucial that objects do not obstruct the view of the turning driver and the oncoming cyclist.

3.5.2 Intervisibility Analysis for Crossing-Path Movements

Crossing accidents occur when cyclists and vehicles intersect at right angles, particularly at intersections without signal control. As introduced in design guidelines, such as RASt in the 2.3.2, road design principles prescribe sight triangles based on ISD to ensure that approaching road users from crossing streets can see each other. This requirement is particularly

critical at unsignalized intersections, where stop- and yield-controlled movements depend largely on drivers' and cyclists' visual perception and decision-making, both of which are strongly influenced by available sight distance [Kilani et al. 2021]

The placement of the sight triangle is determined based on a combination of two factors: whether cyclists are on a priority road or a major road, and whether the conflict occurs at the far side or the near side from the major road users' point of view, as shown in Figure 3.4.

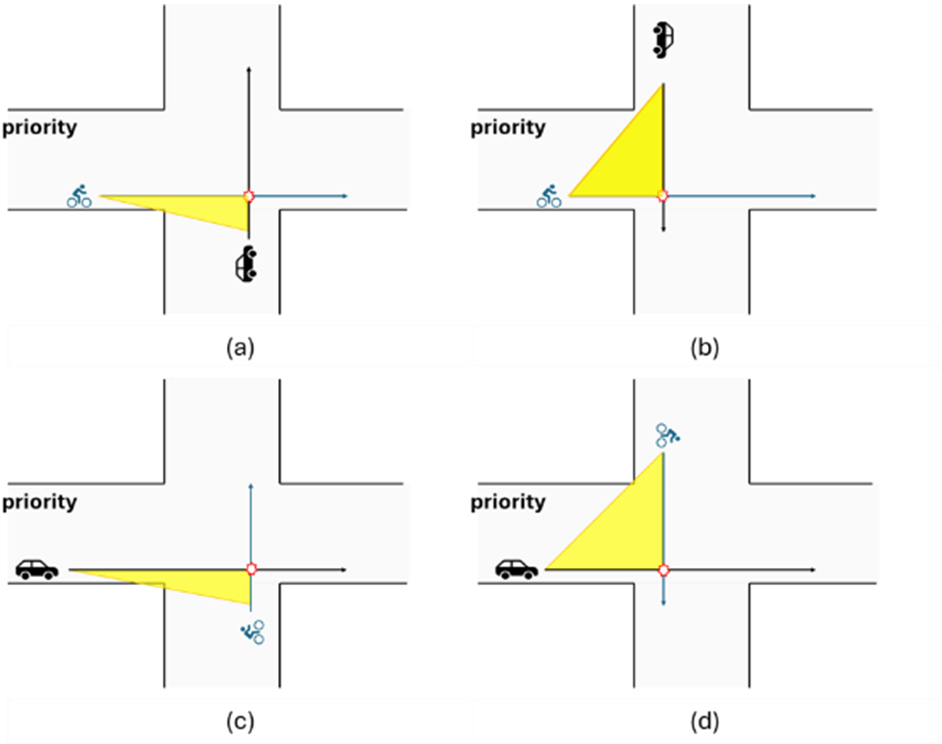

Figure 3.4: Crossing collisions and corresponding sight triangles. Figure (a) and (b) show the case where cyclists are on a priority street, observing the sight triangle with a vehicle entering the intersection from left and right side from cyclist's perspective. Figure (c) and (d) show the opposite case

Another factor influencing the exact dimensions of sight triangles is the design speed of the primary road user and the distance of the stopping or decision-making point on the minor road, as described in 2.3.2. Leveraging 3D data derived from CityGML, supplemented by TIAS and SUMO, this study evaluates the extent to which the prescribed sight triangle is free from visual obstructions.

Although there is a requirement for vertical clearance of 0.8 m to 2.5 m above ground within this triangle in Germany, the analysis is conducted in the form of a mutual visibility assessment, with fixed eye heights of cyclists at 1.5 m and that of drivers at 1.2m. The placement of the stopping or yielding user's decision point is set at 3m back from the edge

of the intersection [StVO2Go 2022]. In a scenario where a motorist is on a minor road, waiting to cross a major road with a cycling lane, the placement of the decision point is 3m back from the center of the cycling lane. Both situations are described in 3.5.

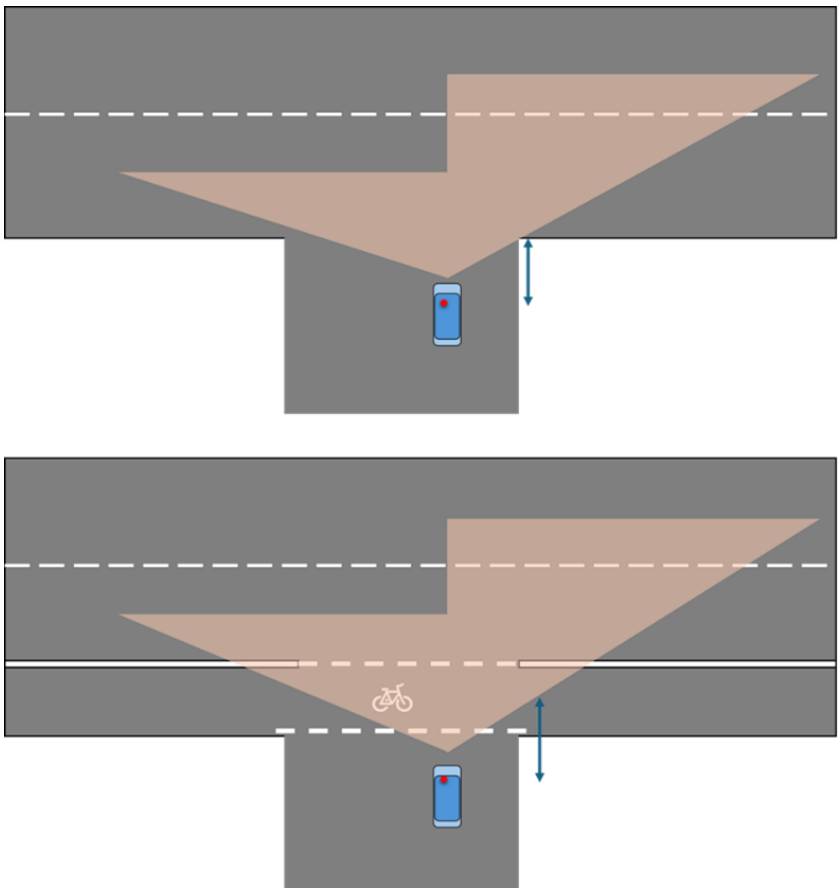

Figure 3.5: The position of observer point with absence and presence of cycling lane on major road

3.6 Quantification Framework

Both intervisibility analyses are carried out under the same environmental settings: each is applied to the scenarios of differing above-ground elements, using the Intervisibility and the Line of Sight (LoS) geoprocessing tool as the primary geoprocessing methods. While they share the same input data and tool, the two analyses differ in the analytical approach used to derive the visibility value and in the type of accidents for which each indicator is valid.

3.6.1 Indicators for Hook Collision

The conceptual workflow of the intervisibility analysis consists of three stages.

In the first stage, conflict points are identified between the driving path and the cycling path, corresponding to right-hook and left-hook collision patterns. Each conflict point represents a potential location where car–bike interaction requires mutual visibility unless special traffic measures, such as signal control, are in place. As discussed earlier, hook conflicts are not always resolved by the controls, even at signalized intersections due to simultaneous greens. Therefore, all types of conflict points present in the scene will be subject to the selection at this point, regardless of the existing control measures. Geoprocessing intersection is used to find the path crossing among driving and cycling lanes as shown in Figure 3.6. The generated conflict points are sorted manually according to its bike-vehicle interaction pattern, referring to driving path and cycling path layers.

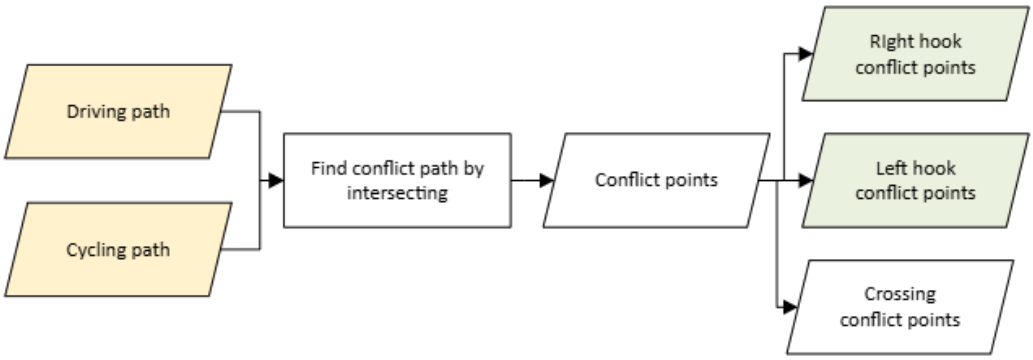

Figure 3.6: Procedures of extracting conflict points among driving and cycling paths. Conflict points are sorted manually into hook accident pattern and crossing conflict pattern

The second stage defines upstream observation zones along both travel paths. The core aspect of safety lies in the early detection of potential conflicts within these upstream segments. For this purpose, segments of sufficient length are delineated to theoretically provide adequate space for perception and reaction. According to the stopping sight distances [StVO2Go 2022], a car traveling at 30 km/h requires approximately 22 m, at 40 km/h about 33 m, and at 50 km/h roughly 47 m of clear sight distance on a level road (0° slope) to come to a complete stop. However, when approaching an intersection with the intention to turn, drivers typically reduce their speed to ensure a safe turning maneuver. Consequently, the effective sight distance required in such situations is shorter than the stopping distance based on design speed. Applying a conservative buffer, upstream extraction distances of 40 m for roads with a speed limit of 50 km/h and 40 km/h are assumed to represent the critical visibility ranges for assessing intervisibility.

Along these segments, observer points and target points are generated at short, regular intervals and elevated to the respective eye heights of drivers and cyclists, thereby reflecting realistic human perception conditions. The selected interval is 0.5 m for both road users and cyclists' and drivers' eye heights are assumed at 1.5 m and 1.2 m respectively according to German road design guideline [Forschungsgesellschaft für Straßen- und Verkehrswesen (FGSV) 2006]. The flow chart for the case of right hook intervisibility is shown in Figure 3.7.

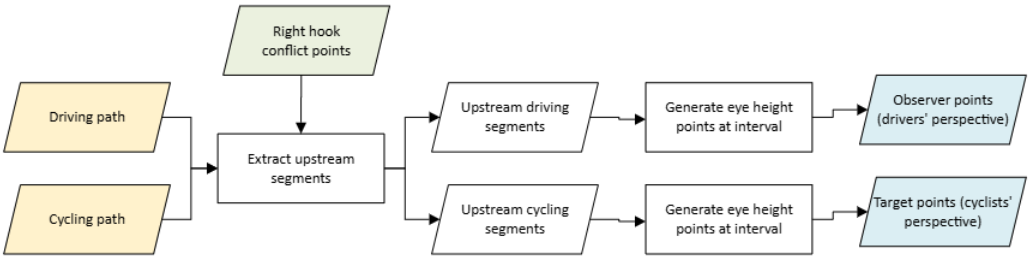

Figure 3.7: Procedures of generating observer and target points from extracted driving and cycling segments

The third stage involves applying the Line of Sight (LoS) analysis by generating sightlines between each observer–target pair linked to a conflict point. Specifically, from every observer point associated with a given conflict point, sightlines are drawn toward all corresponding target points of the same conflict point. Since both observer and target points are created at 0.5 m intervals, the total number of observer–target pairs per conflict point can be expressed as:

$$\text{Number of pairs} = (\text{biking upstream segment length}) \times (\text{driving upstream segment length}) \times 4$$

Through LoS analysis, each sight line is classified as either obstructed or unobstructed in each scenario with different obstruction input in the scene. For every observer point, the number of visible and blocked sightlines is counted and recorded in the sight line's attribute table. These results are then aggregated per conflict point to calculate a visibility ratio for each conflict, an approach similar to that of González-Gómez et al. (2022). This ratio is subsequently mapped back onto the input upstream segments. The flowchart is described in Figure 3.8.

All the procedures after generating sight lines involved in this stage are repeated under different obstruction data input, namely vegetation, city furniture, buildings and parked vehicles. The yielded values are named Blocked Rate (BR) which serves as the quantified intervisibility indicator representing the safety associated with the identified conflict.

The illustrative description in Figure 3.9 outlines the step-by-step procedure up to the intervisibility assessment. The subsequent processes involve counting the number of blocked

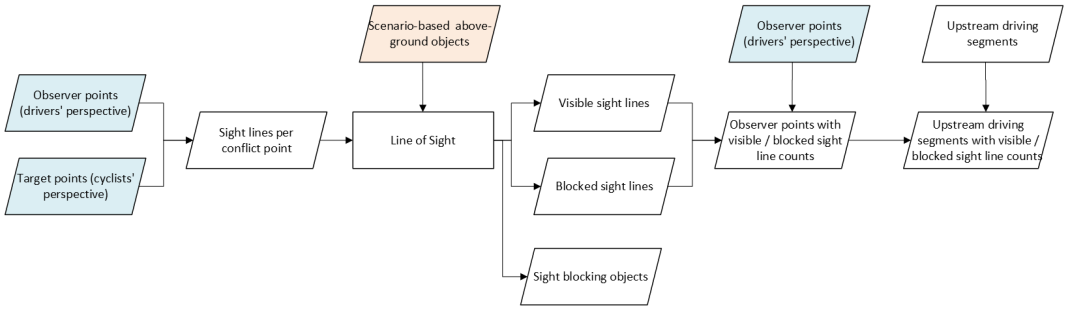

Figure 3.8: Procedures of Line of Sight analysis and aggregating sight line block counts for hook conflicts

(red) lines and uninterrupted (green) lines, followed by calculating the blocked rate, by dividing the number of blocked lines by the sum of both lines.

3.6.2 Indicators for Crossing Collision

Unlike the intervisibility analysis for turning movements, the viewshed analysis is based on the regulatory sight triangle defined in road design guidelines. It investigates whether a clear field of view is maintained within this framework. The conceptual workflow largely parallels that of the intervisibility analysis, with key methodological differences. The first step is to identify conflict points corresponding to near-side and far-side collision patterns, while also distinguishing whether the road user of interest is approaching from a priority road or a side street. This classification informs the subsequent definition of the sight triangle. Three elements form the sight triangle: the decision point position of a user on the minor road with stop- or yield control, the conflict point, and the location of the other user on the major road at a distance equal to the Intersection Sight Distance (ISD), which is determined by the design speed of the major road. In the next step, the long leg of the sight triangle is extracted from the upstream segment of the major road, while the short leg is fixed at the stopping position of the minor road user, serving as the observer location. From the upstream segment, equally spaced target points are generated and vertically elevated to the level of the corresponding road user's eye height. The observer position is also elevated to eye height (1.2 m for drivers, 1.5 m for cyclists) but remains fixed, as its dynamics are not considered. Finally, sightlines are constructed between the fixed observer and each target point within this sight triangle, with a discretely represented road user's point of view on a major road. For each conflict point, the number of visible and invisible sightlines is counted, and a visibility ratio is calculated. This ratio, calculated around the stopping point, is then assigned to the path intersecting with the point, returning the quantified visibility indicator value to the original CityGML line layer. The flowchart is shown in Figure 3.10.

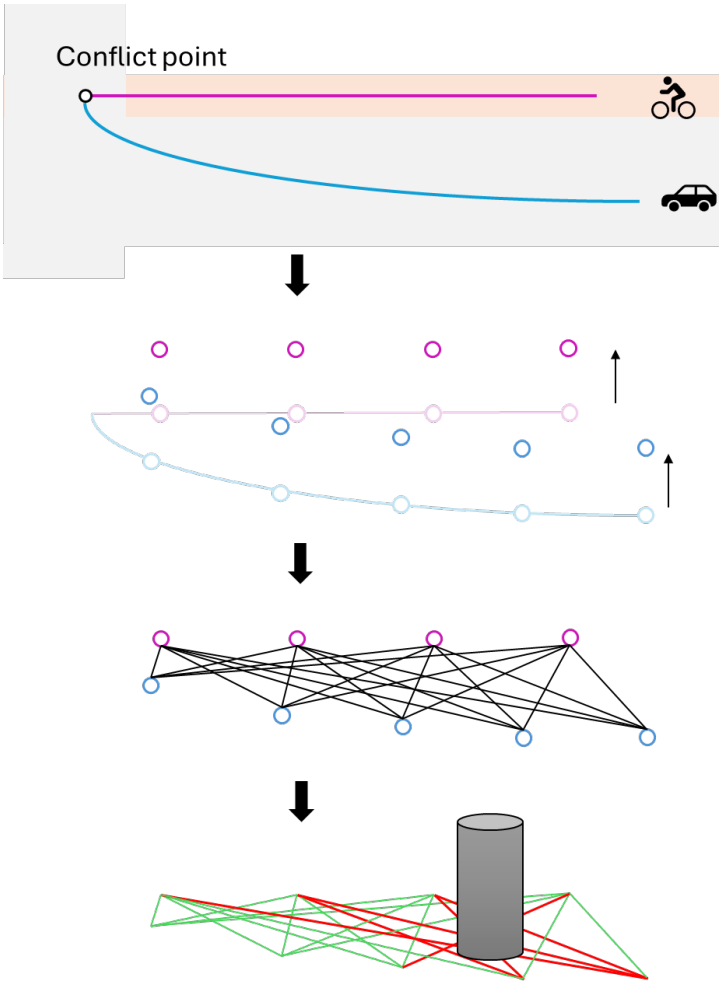

Figure 3.9: Illustrative steps from upstream path extraction to intervisibility assessment. The extracted upstream segments are used as base to generate points at a certain interval and these points are generated to users' eye height. Sight lines are generated connecting the corresponding points and then intervisibility analysis with obstruction is conducted.

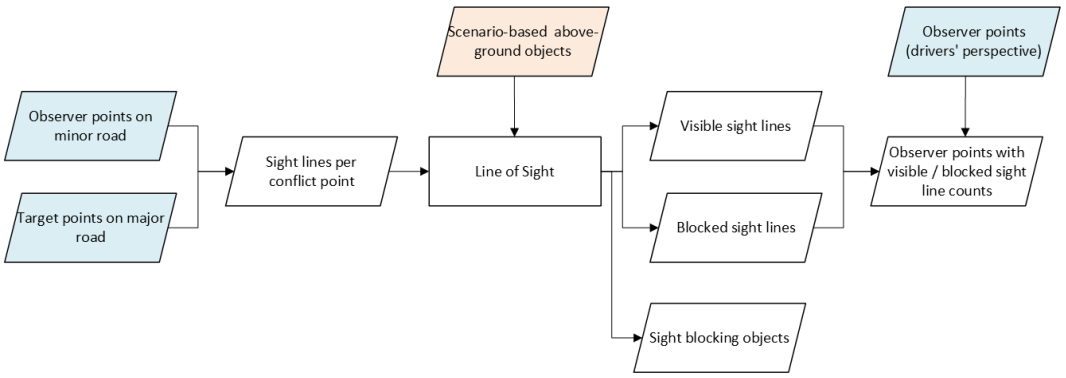

Figure 3.10: Procedures of Line of Sight analysis and aggregating sight line block counts for crossing conflicts

3.7 Visibility Obstruction Identification

The identification procedures of sight line blockage causes are built upon the quantification procedure, as the tool Line of Sight can optionally generate a point layer where all the IDs are stored each time a sight line between observer and target is cut in the way [Esri 2025]. The identification processes transform the geometric output generated by LoS into a spatial understanding of the obstruction causes, playing a crucial role in connecting the concrete physical elements within the 3D urban model and the lack of visibility.

The IDs of obstructing objects are summarized for each conflict point, allowing the sources of obstruction to be systematically associated with specific collision types and intersection layouts. This aggregated output enables the interpretation of the visibility indicator within both its spatial and semantic context. The frequency of sightline obstructions linked to a given conflict serves as an indicator of the severity of visibility reduction. By connecting the cause, extent, and spatial distribution of these obstructions, the results gain diagnostic value within the overall analysis framework. For instance, cases where the visibility of right-turning drivers toward cyclists is frequently hindered by parked vehicles, or where buildings located at intersection corners consistently increase blockage ratios, reveal recurring patterns of intervisibility reduction characteristic of particular collision types by particular elements. Such insights provide a sound foundation for design-oriented safety improvements by clarifying which elements cause obstructions and to what extent they do so. This understanding enables designers and urban planners to prioritize effective measures that enhance visibility and mitigate potential conflicts.

4 Implementation

4.1 Data Preparation and Preprocessing

Before conducting the visibility analysis, several preprocessing steps were necessary to ensure the datasets were suitable for analysis. These procedures aimed to verify the completeness of spatial coverage, the geometric accuracy of each layer, and the availability and consistency of semantic information required for this thesis.

The following sections describe the verification and quality assessment processes applied to the static obstruction data from CityGML, the lane models, and the TIAS parking data, as well as the subsequent modifications, filtering, and data enrichment steps performed when necessary. It was essential to distinguish between datasets that were directly usable in their raw form and those that required preprocessing. This distinction enabled a precise evaluation of the degree of data preparation required and the extent to which automated workflows could be applied with minimal manual intervention.

4.1.1 TIAS and Parking Data

The TIAS data, generated through an automated segmentation model developed by DLR, is provided in a 2D polygon format, in which areas identified as having "parking" as their primary or secondary use are extracted. Each polygon represents not only the tight-fitting footprint of individual detected vehicles but rather a slightly broader area encompassing the parkable space. This is especially true when multiple vehicles are detected along a longitudinal roadside segment, as the resulting polygon typically outlines the entire stretch of space occupied by or suitable for parked vehicles. As a result, the dataset indicates areas suitable for parking rather than the precise footprints of individual vehicles (Figure 4.1). The number of vehicles that can be accommodated within each polygon is specified in the corresponding attribute table.

The polygons do not necessarily have a rectangular shape typical of individual vehicles as they represent parking areas and not detected vehicles themselves. Therefore, no gaps are present between vehicles parked in a longitudinal arrangement when the vehicles are close to each other. This raw TIAS-derived data were used as a basis to construct 3D blocks representing potential visibility obstructions through extrusion by the height of 1.8m, heigher

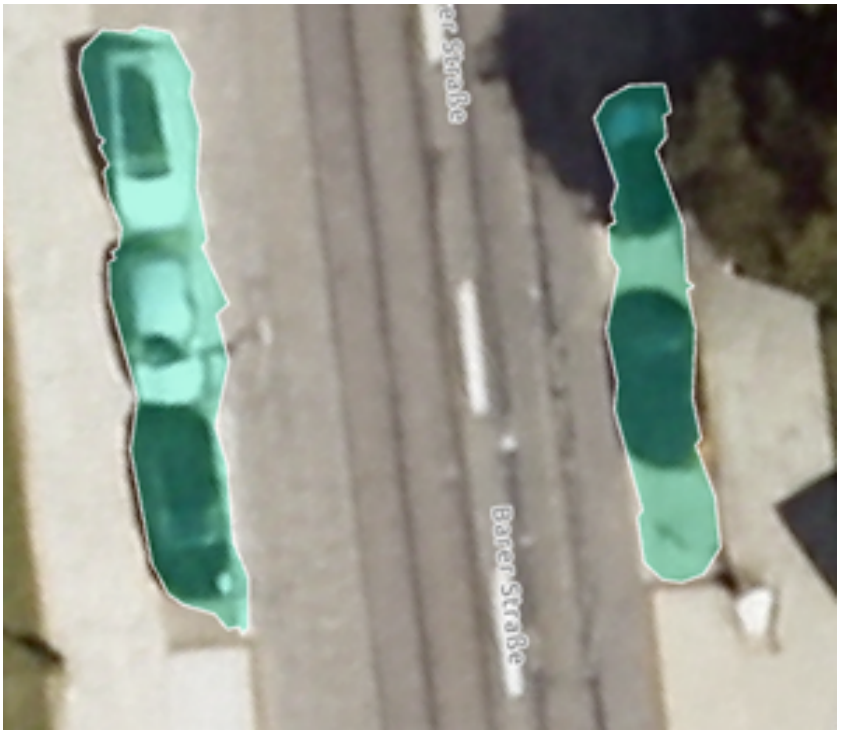

Figure 4.1: TIAS parking area extraction in longitudinal sequences

than the assumed height of eyes of drivers (1.2m) and cyclists (1.5m). These blocks function as virtual walls within the analysis environment. This approach inevitably covers a larger volume than the actual vehicles would, as multiple adjacent vehicles are often merged into a single continuous block, thereby eliminating potential sight gaps between cyclists and drivers. Practically, gaps in parked vehicles should depend on the time of the day. Nevertheless, this generalization is considered practically appropriate for representing a worst-case or conservative scenario, in which larger vehicles such as buses or trucks could obstruct visibility. An example of the scene with parked vehicles is in Figure 4.2.

For both the CityGML-derived obstruction layers and the TIAS-derived parking vehicle layers, the Line of Sight tool in ArcGIS requires a single obstruction feature layer as input. Therefore, all obstruction datasets needed to be merged into a unified layer to perform analyses for both Scenario 1 and Scenario 2. Initially, separate analyses were conducted for individual obstruction types,CityFurniture, Buildings, and Vegetation,to examine their respective impacts on visibility. Subsequently, these layers were combined into a composite obstruction layer for integrated analysis. In Scenario 2, the extruded TIAS-based 3D vehicle blocks were also incorporated into this unified layer, ensuring that all relevant visibility barriers were represented in the analysis.

Figure 4.2: TIAS parking area extrusion

4.1.2 Lane Model Preprocessing

CityGML transport layers such as `TrafficArea` and `TrafficLine` do not natively provide semantic attributes like designed speed or road usage type in their attribute tables, even though this information exists in the original GML file as "generic attributes" attached to each lane. To make these attributes directly usable, data transformation was performed in FME Workbench so that both road usage type and speed are represented as dedicated table columns (see Figure 4.3).

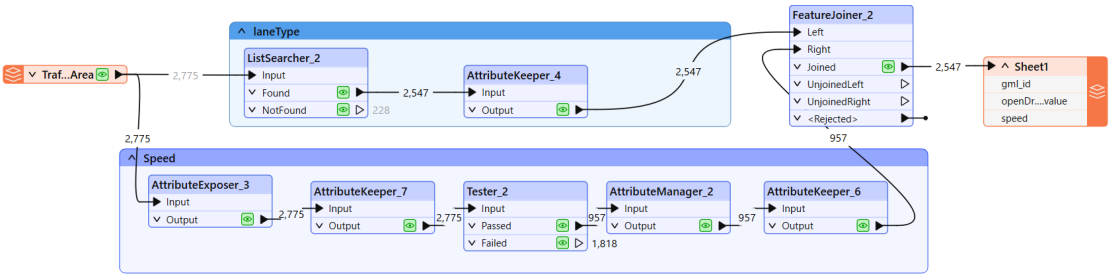

Figure 4.3: FME workbench geoprocessing turning speed and road usage type into visible attributes

One of the geoprocessing steps involved is type extraction: the `ListSearcher` transformer was applied to the `TrafficArea` layer to identify the lane usage type within the `genericAttribute` field (Figure 4.4). In CityGML datasets converted from OpenDrive, lane usage is stored as a string variable under the attribute `opendrive_lane_type`, which includes

values such as “DRIVING”, “BIKING”, “SIDEWALK”, “PARKING”, and “SHOULDER”.

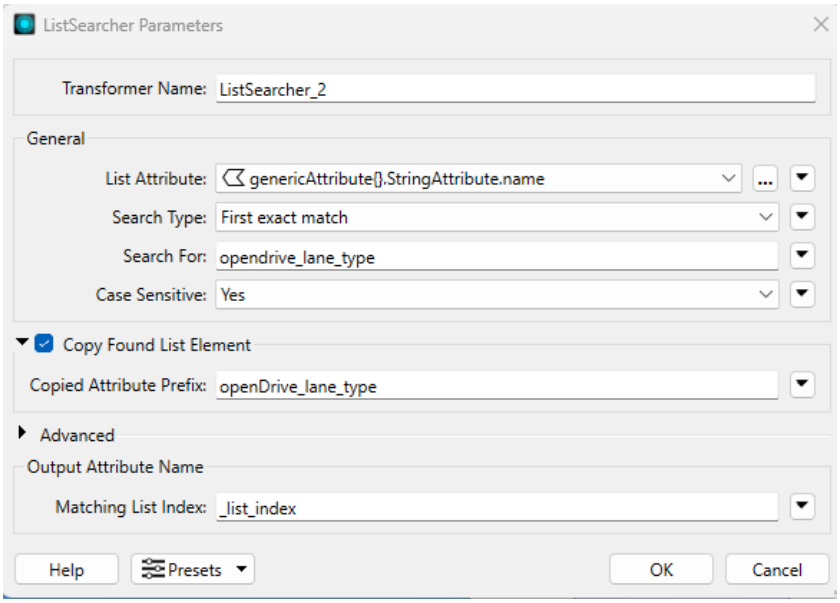

Figure 4.4: FME workbench ListSearcher parameters

The other geoprocessing step is speed extraction. To retrieve the designed speed, the `AttributeExposer` transformer is used. Each feature in the GML file contains multiple generic attributes, but their order varies by feature. Since attribute indices are assigned sequentially (e.g., `genericAttribute(1)`, `genericAttribute(2)`), the speed value appears under different positions across features. These positions were identified through manual inspection, and the corresponding attributes were explicitly exposed in the workbench (see Figure 4.5). Furthermore, subsequent transformers filter out invalid entries and retain only relevant attributes. The processed data is then written back into the CityGML file with enriched semantic information, enabling more direct use in later analyses.

The output of the geoprocessing in FME Workbench is generated in spreadsheet format (MS Excel), where the `gml_ID` serves as a unique identifier. This ID can be used as a key to join the resulting table, which contains the newly extracted speed and type attributes, with the existing `TrafficArea` or `TrafficSpace_line` layer.

4.1.3 Driving and Cycling Path Preprocessing

Once the updated transport layers were added to the scene, lines were distinguished according to usage, and their missing parts were completed. In this process, cycling and driving segments were extracted from the `TrafficLine` layer based on their usage type. In cases where connections were missing, they were manually corrected with reference to map ser-

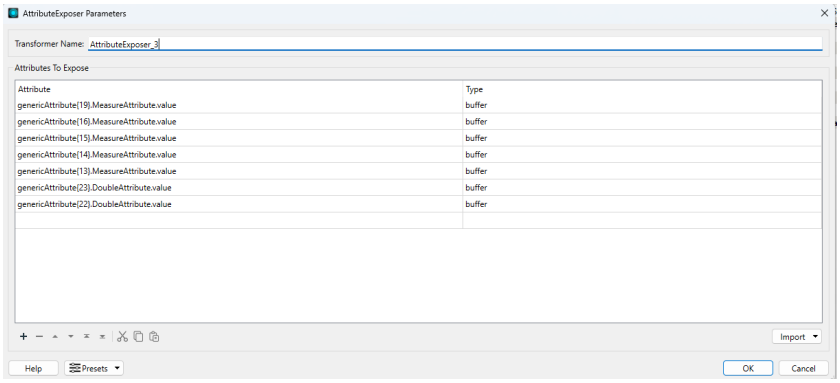

Figure 4.5: FME workbench AttributeExposer parameters

vices such as Google Maps, Google Earth, and the built-in aerial imagery background, as shown in Figure 4.6.

Figure 4.6: Manual editing of the missing cycling path

Path modifications were conducted under the following conditions:

- A cycling lane is clearly visible in aerial imagery but missing in the lane model.
- A driving lane is incorrectly labeled as a cycling lane, or vice versa.
- Adjacent line segments are discontinuous, although they should be connected in reality.
- An impossible path is present, such as a driving lane drawn in the wrong direction on a one-way street.

The intervisibility analysis is susceptible to the positional accuracy of path geometries, as these serve as the basis for generating virtual eye positions. Therefore, any modification or addition of paths was performed only when explicit aerial imagery was available, either

from the built-in Esri basemap or from DOP (digitally orthophotographed) aerial images imagery, which also served as the reference for generating the TIAS segmentation results.

Although numerous missing or misclassified paths were identified during the inspection of the lane model, not all were subject to correction, as the primary objective of this thesis is to develop automated analytical processes. Modifications were made according to the above criteria, where the correct path is clearly visible in the imagery. Adding new connections was also not thoroughly done, as the output of the visibility analysis should eventually be reflected in the CityGML transportation module. Moreover, the incompleteness or inaccuracies observed in the dataset are not inherent to the CityGML Transportation Module itself but specific to the dataset employed or to OpenDrive, based on which CityGML was generated. Consequently, extensive manual modifications to complete the driving and cycling paths across the entire study area were deliberately avoided.

4.1.4 Conflict Points Classification

Conflict points are generated at the intersections where the segregated driving lane layer and the cycling lane layer overlap. The *Intersect* geoprocessing tool is applied to identify these overlapping points, which are then manually classified according to the type of interaction between cyclists and motorists. A simple sketch illustrating the manual sorting procedure is provided in Figure 4.7.

Among the conflict points identified at each intersection, the right-hook and left-hook types (top two) are categorized as *hook conflict points*, while near-side and far-side crossing types (bottom two) are classified as *crossing conflict points*. The classification rules are defined as follows:

- When the cycling path and driving path share the same street prior to the conflict, a *hook collision* occurs.
- When the cycling path and driving path originate from two different streets that intersect, a *crossing collision* occurs.

Crossing conflict points require additional sorting based on the intersection control measures and the road hierarchy (major vs. minor road):

- **Traffic signal present:** Conflicts are assumed to be resolved by signal control; therefore, crossing collisions are excluded from the analysis. It is assumed that traffic signals in the study area operate with simultaneous green phases for turning vehicles and straight-moving cyclists, meaning that right-hook and left-hook collisions were still examined regardless of signal presence.

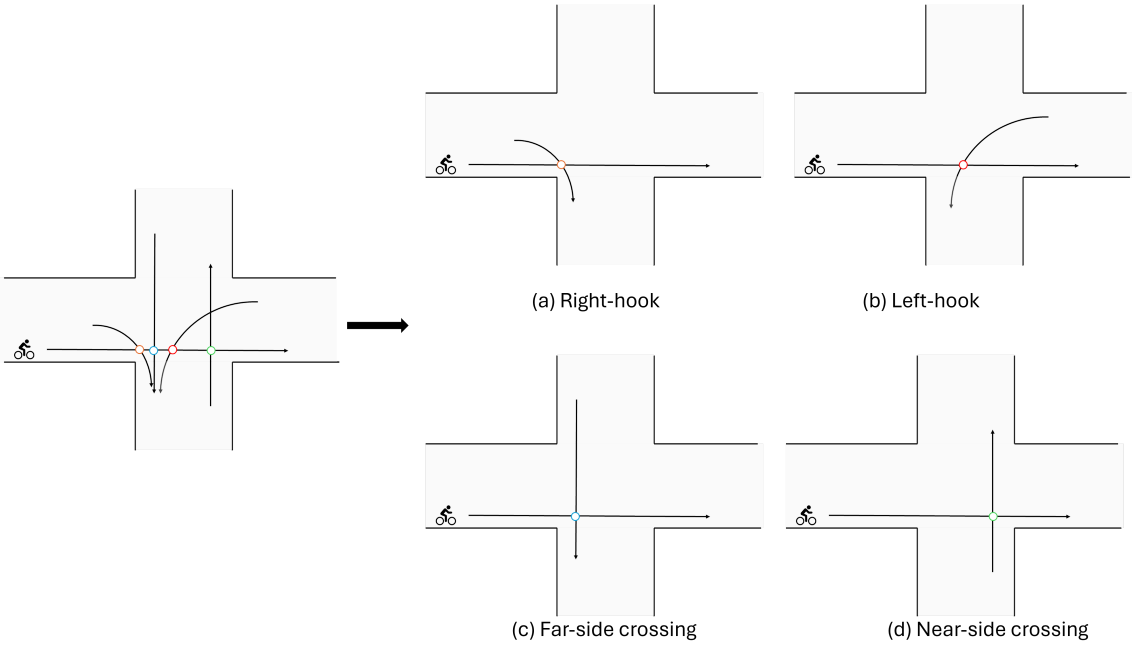

Figure 4.7: Manual classification of the conflict points based on hook and crossing type. Near-side and far-side are decided from driver's point of view regarding its interaction with a cyclist

- **Traffic signal absent:** The major and minor roads were distinguished, as unsignalized minor roads typically include stop or yield signs giving priority to users on the major road. This classification was verified using Google Maps Street View.

4.2 Intervisibility Analysis for Hook Collisions

The conflict points labeled as hook collisions, along with the corresponding original driving and cycling paths used to generate them, serve as the foundation for the subsequent analytical procedures. At this stage, the available data must be geoprocessed and transformed into a format suitable for use as input in sightline construction, which is required for executing the Line of Sight and Intervisibility tools. The essential inputs for generating sightlines consist of an observer point and a target point. Several custom `arcpy` algorithms were developed to trace a defined distance upstream along both the driving and cycling paths, while preserving the attribute information that links each extracted segment to its corresponding conflict point.

4.2.1 Upstream Path Extraction

The first step in the intervisibility analysis for turning or hook accidents is to extract upstream segments from conflict points, which serve as anchor nodes linking the cycling and driving paths. Upstream segments are traced within predefined distances from each conflict point. For cycling paths, a distance of 25 m is applied, based on the assumption that cyclists travel at 30 km/h, which corresponds to the minimum sight distance required under German standards, accounting for reaction time and deceleration [Omer Malak and European Cyclists' Federation (ECF) 2022]. For motorists, an upstream distance of 40 m is chosen, reflecting the typical speed environment on urban residential streets within densely built areas, as explained in chapter 3.

The extraction process was implemented in a Python script executed within ArcGIS. The operation began by connecting the line segment to each conflict point, identifying its travel direction, and then searching for the next upstream connection using a graph-based approach. For each conflict point, the script determined the intersecting line segment, calculated its position along the polyline, and traced backward until the predefined distance was reached. If the distance extended beyond the current segment, the procedure continued along the connected segment according to the network's topology. All traversed segments were stored as part of a polyline collection, and the final output consisted of two layers: one containing the raw fragmented segments and another with merged upstream paths. Figure 4.8 illustrates the network before and after this operation.

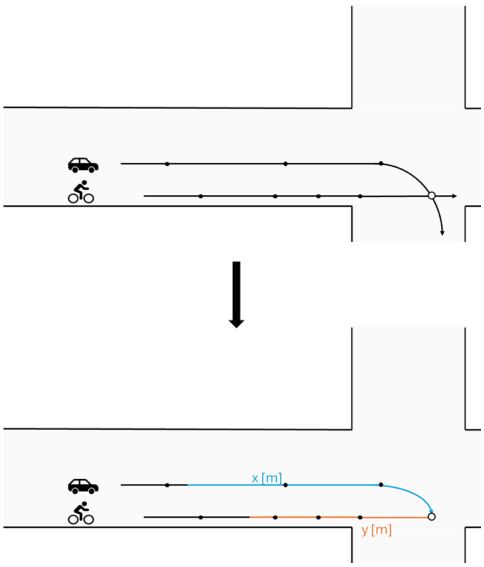

Figure 4.8: Tracing upstream segments from right-hook conflict point

These extracted upstream segments of both cycling path and driving path are uniquely

tied to the conflict point they share, ensuring a one-to-one correspondence. The output is segmented or merged along the upstream path of both the biking path and the driving path, as shown in Figure 4.9.

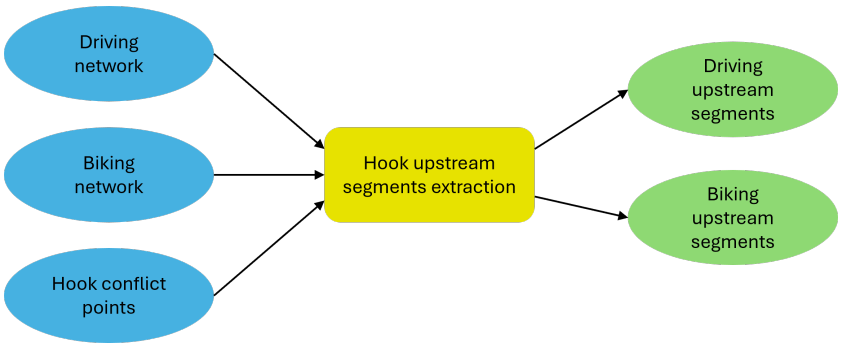

Figure 4.9: ArcPy process of generating upstream segments. Input data are the identified hook-pattern conflict points, CityGML-derived driving and cyclnig path.

The flowchart of the procedures included in the code is shown in Figure 4.10

The algorithm operated based on the orientation information stored in the input line data. However, several cases of orientation mismatch resulted in the premature termination of the upstream tracing. To address this, a debug-enabled version of the code was developed, allowing the script to output messages when tracing could not continue before reaching the predefined distance. When an orientation mismatch was detected, the input data were manually corrected by reversing the direction of the affected line. Additionally, due to the algorithm's simple structure, it was unable to continue tracing when a path split into multiple branches (or when several paths merged into one during upstream tracing). In such cases, manual selection of the appropriate upstream path was required. When multiple upstream options were available, the path aligned with the same street as the preceding segment was prioritized. However, this situation rarely occurred, as most merging points or intersections were located more than 40 meters apart.

4.2.2 Observer and Target Definition and Sight Line Generation

The upstream trajectories generated by the script serve as the basis for creating observer and target viewpoints, representing drivers and cyclists, respectively. To establish sightlines between them, the trajectories must be discretized into a sequence of equally spaced observer and target points. This is achieved using the *Generate Points Along Lines* tool in ArcGIS Pro, with the upstream trajectories as input and an interval distance of 0.5 m. While González-Gómez et al. (2022) applied a spacing of 1.0 m, the interval in this study was reduced to 0.5 m, as a higher point density provides more precise visibility estimations, provided that

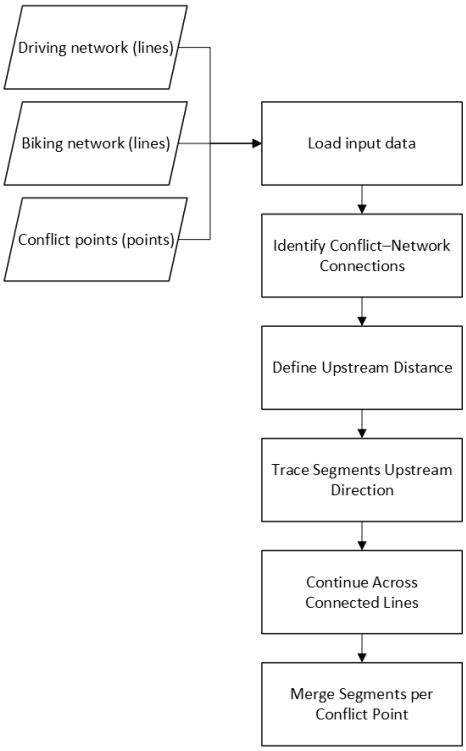

Figure 4.10: Script details of upstream segment extraction process

computational resources allow. The resulting points represent the horizontal positions of the observers' and targets' viewpoints. These points are then elevated using the *Elevate Points* tool, which assigns realistic eye heights by converting the Z-coordinate. Following German guidelines introduced in subsection 2.3.2, cyclists are assigned an eye height of 1.5 m, while drivers are assigned 1.2 m.

After establishing observer and target points, 3D sight lines between all observer–target pairs anchored to the same conflict point ID are generated using the *Construct Sight Lines* tool. The continuity of the created sight lines without interruption will be assessed in the subsequent Line of Sight and Intervisibility analysis. The procedures involved in preparing sight lines are modeled using ModelBuilder and are described in Figure 4.11.

4.2.3 Intervisibility Analysis and Output Generation

Once sight lines connecting the drivers and cyclists are defined, the next step is to assess whether these lines are interrupted by the presence of 3D objects in the chosen urban scenario. The *Intervisibility* tool is applied to all the generated sight lines with 3D objects as input to the environment. The tool produces a binary visibility result, showing visible as

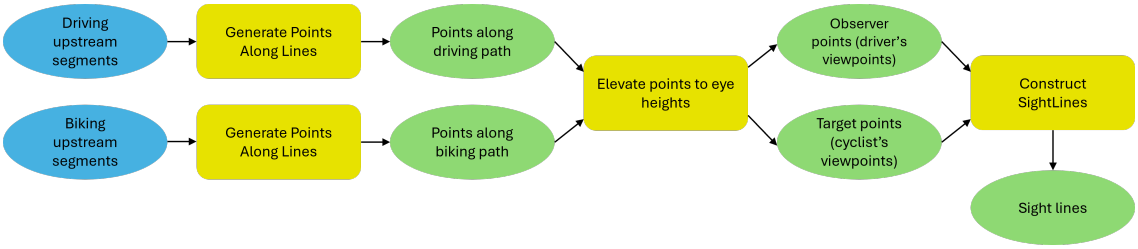

Figure 4.11: Script details of sight line generation process from the extracted paths. Generate Points Along Lines geoprocessing tool available in ArcGIS is used to generate interval points. An Arcpy script is included to process the generated point into z-enabled points at respective users' eye height. Custom-made Constructing Sight Lines tool is then used to build lines connecting observer and target points while keeping the conflict ID data.

"1" and blocked as "0", in a new field of the attribute table for the sight line feature layer. To aggregate the results per observer station, *Summary Statistics* is used to count the number of unblocked and blocked sight lines that departed from the same point. These numbers are used to calculate the blocked rate values. Then the values in this summary table are returned to the points tied with a shared ID using the *Join* tool. To transfer these attributes to the CityGML-derived driving line segments, the previously created driving upstream segment layer is invoked, which is enriched with the calculated values and conflict point IDs as anchors for the joining process. An example of this metric is shown in Figure 4.12.

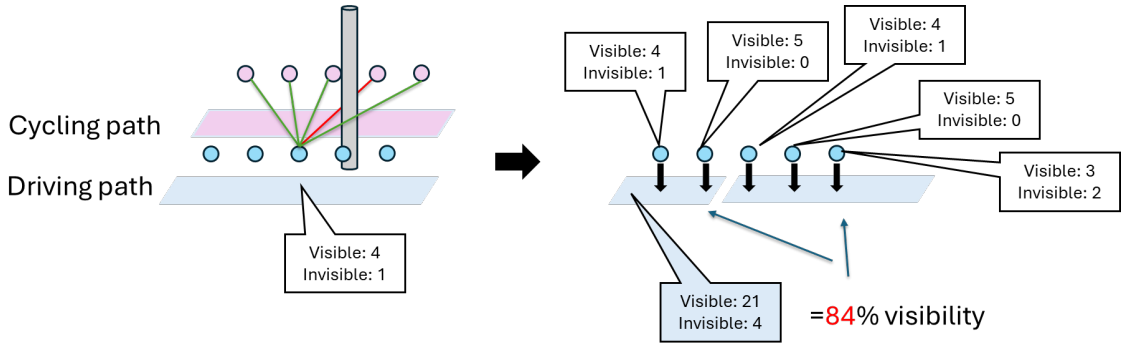

Figure 4.12: Assigning blocked rate calculated per conflict point to corresponding driving paths

The counted visible sight lines and blocked lines are used to generate a normalized metric for facilitating interpretation, defined as

$$\text{Blocked rate} = \frac{\text{Blocked sight lines}}{\text{Blocked sight lines} + \text{Visible sight lines}} \tag{4.1}$$

This measure represents the proportion of blocked sight lines out of the total sight lines associated with each upstream segment of the observer. This indicator ranges from 0 to 1, with higher values indicating a greater likelihood of visibility obstruction between cyclists and motorists. The first half of the procedures in ModelBuilder for intervisibility analysis is shown in Figure 4.13.

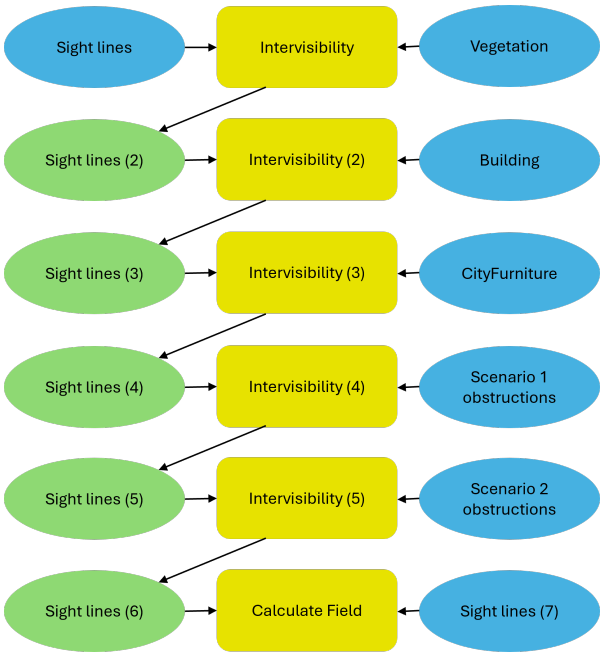

Figure 4.13: Intervisibility analyses to count the visible sight lines with different obstruction layers as input. Scenario 1 includes the three CityGML layers together. Scenario 2 includes parked vehicles in addition to scenario 1 obstructions. Calculate Field tool is used to subtract scenario 2 from scenario 1 to understand parked vehicles' exclusive impact on visibility

Each time the Intervisibility tool runs, it adds a new field in the input sight line attribute table with binary output. The output blocked rate value calculation model is shown in Figure 4.14.

The output from the *Intervisibility* tool provided only a binary judgment of whether each sight line was obstructed or not and did not indicate which objects caused the obstruction. While this output helped calculate obstruction-category-based sight line blockage rates, it did not allow object-level attribution. Since another objective of this analysis was to identify specific blocking objects (by their IDs) and to quantify the extent to which each object interfered with sight lines, the *Line of Sight* tool was also employed. This tool differed from the *Intervisibility* tool in that it required an elevation surface as an additional input and produced two output layers: one containing sight lines segmented at obstruction points, and

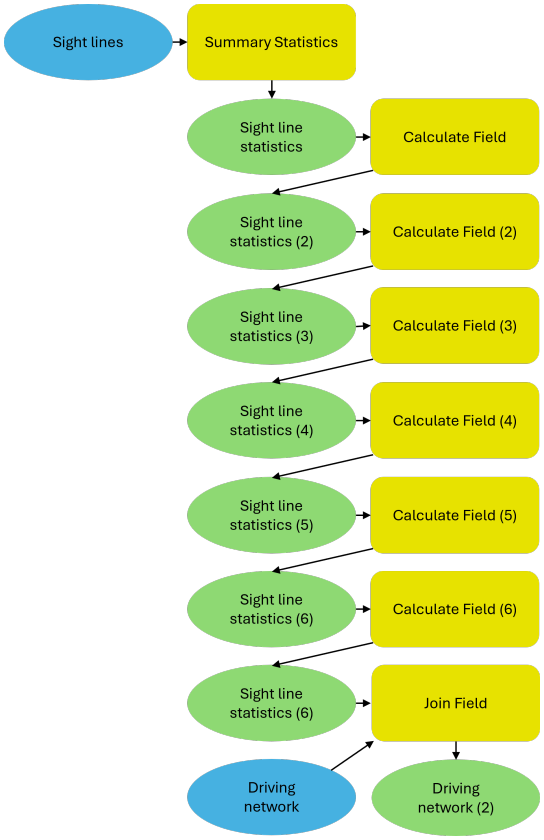

Figure 4.14: Calculation of the rate of blocked sightlines out of all the sightlines corresponding to the same conflict point

another consisting of point features representing all identified interruption points. Of these two outputs, the point layer was used for further calculations. Each point feature in this layer retains attribute information indicating the source sight line from which it originated. Because sight lines were associated with conflict point IDs, the obstruction points could also be indirectly linked to the corresponding conflict point. The blockage rate was calculated in the same manner as in the category-based analysis, using the total number of sight lines as the denominator and the number of obstruction points tied to the same sight line source as the numerator. The ModelBuilder procedure used for this process is shown in Figure 4.15.

4.2.4 Output Structure

The results of the first analysis (*Intervisibility*) were presented in a table showing the sight line blockage rates caused by different obstruction categories, including vegetation, city furniture, and buildings (Scenario 1), as well as these three categories plus parked vehicles (Scenario 2), and the subtraction of Scenario 2 minus Scenario 1. A scenario with parked

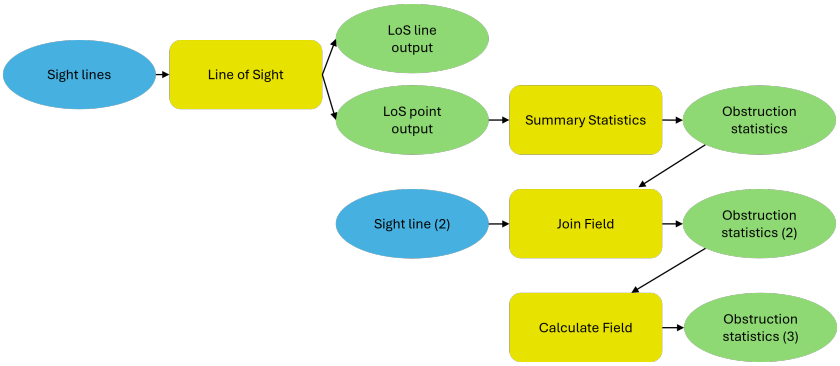

Figure 4.15: ModelBuilder workflow for Line of Sight (LoS) analysis, summarizing obstruction object IDs and the degree to which they contribute to visibility blockage.

vehicles only was not included, as it would be uninformative to measure blockage caused by parked vehicles when one or more static objects already obstructed the same sight lines. The focus of this research lies in identifying the visibility reduction attributable solely to parked vehicles; therefore, their effect was derived by subtracting Scenario 1 from Scenario 2.

The identification of individual obstruction points, however, remained meaningful in the case of parked vehicles. Consequently, the input configuration for the *Line of Sight* analysis differed from that of the *Intervisibility* analysis. The *Line of Sight* tool used only individual layers as input, as the primary objective was to locate specific features that blocked sight lines rather than to obtain category-based blockage statistics.

The outputs of both analyses were summarized in tabular form. The first analysis provided sight line blockage rates attributed to obstruction types such as buildings, vegetation, and traffic signs, while the second analysis produced blockage rates associated with individual obstruction object IDs. Together, these results enabled a comparative assessment of the impacts of obstruction across different conflict types, offering insights into which urban elements most significantly affect cyclist–driver intervisibility within the study area.

4.3 Intervisibility Analysis for Crossing Collisions

The overall procedure in this analysis followed a similar pattern to the previous one. The main difference lay in the upstream path extraction distance for road users on major roads, which was derived from German traffic regulations, and in the determination of static observer points representing the viewpoints of road users on minor roads.

4.3.1 Observer and Target Definition and Sight Line Generation

The placement of these static observer points followed a distinct logic and algorithm. When a driver on a minor road was approaching a major street with a single cycling lane on the near side, the yield or stop point was positioned 3 meters behind the conflict point, as illustrated in the left panel of Figure 4.16. The same distance was applied when two cycling lanes were present (right panel), each corresponding to one direction of travel. When the script generated the yield or stop points, the corresponding conflict point ID was stored as an attribute of the observer point. If one observer point corresponded to more than one conflict point, the IDs of both were stored. In cases where only a far-side cycling lane existed, the yield or stop points were manually corrected at 3 meters from the edge of the intersection. The automation of detecting intersection edges was not implemented separately.

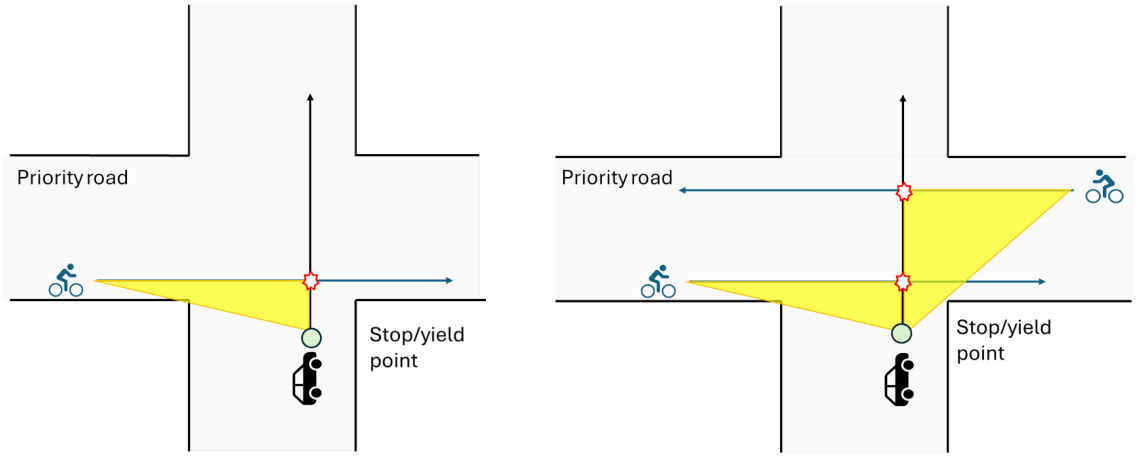

Figure 4.16: Illustration of situation where a vehicle intends to cross main street with one or two cycling lane

The following ModelBuilder workflow was designed to identify the yield positions along driving paths on minor roads and to extract 30 meters of upstream segments from cycling paths. The upstream extraction script was executed twice. The first execution extracted the specified distance and checked whether multiple conflict points were present within the extracted segment. In cases where a driving path crossed two cycling lanes within a short distance, the upstream extraction originating from the downstream (far-side) conflict point could extend beyond the upstream (near-side) conflict point. When such a condition was detected, the observer point was placed 3 meters ahead of the upstream conflict point, before entering the intersection, rather than within it. The Model Builder in Figure 4.17

The conceptual logic is described in the flowchart shown in Figure 4.18.

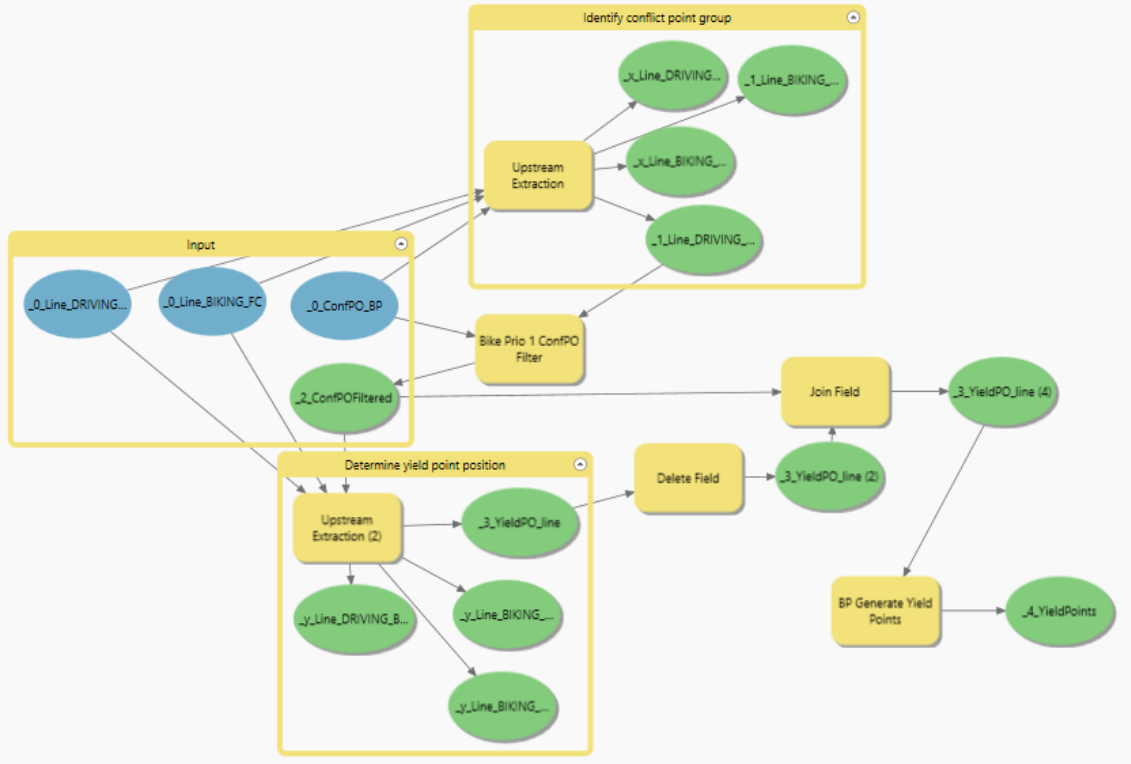

Figure 4.17: ModelBuilder procedure to group conflict points when they intersect with the same path from the minor street, and to place observer (yield/stop) point

4.3.2 Intervisibility Analysis and Output Generation

The procedure in this phase followed a similar structure to that of the hook visibility analysis. The main difference was that, instead of generating multiple observer points and target points for each conflict point, a single observer point corresponded to multiple target points created at defined intervals along the extracted path. The ModelBuilder workflow used for this process is shown in Figure 4.19.

The subsequent visibility analysis algorithm and the process leading to the quantified indicator values followed the same logic as in the hook collision analysis; therefore, the same Model Builder was used to generate these results.

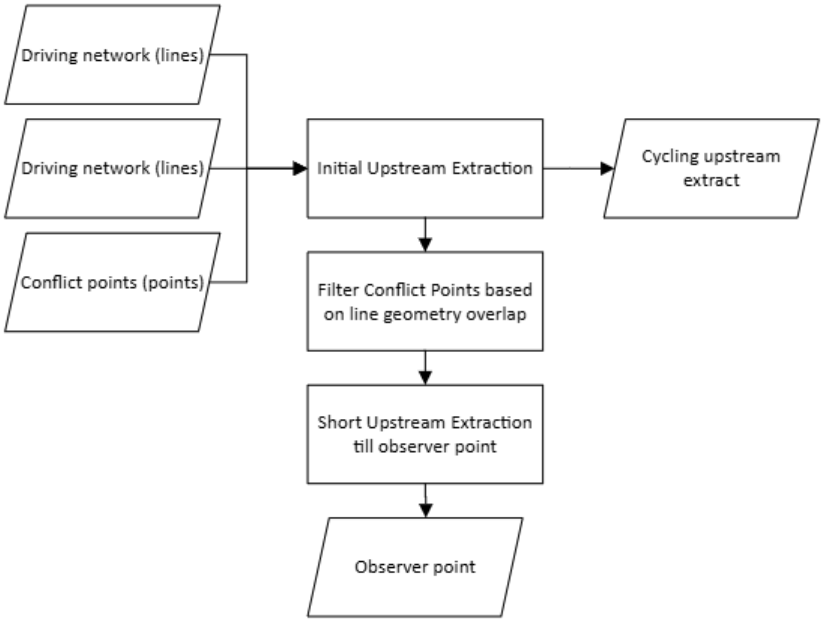

Figure 4.18: Logic flow included in the Model Builder Figure 4.17

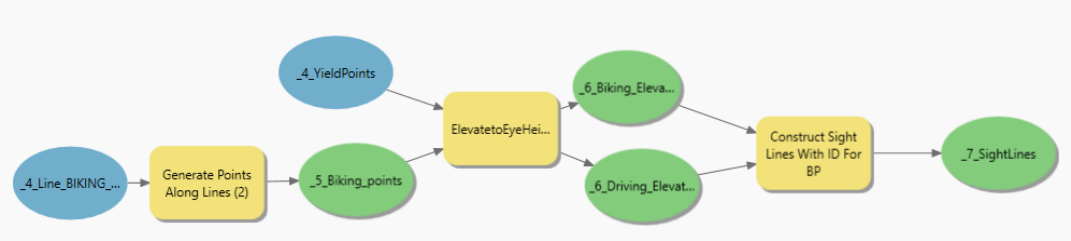

Figure 4.19: ModelBuilder workflow to generate sight lines between an observer point and discrete target points on the priority street

5 Results

5.1 TIAS-derived Data Comparison with CityGML Data

A comparison was conducted between the TIAS-based and CityGML-based datasets to evaluate the completeness and suitability of the TIAS data for visibility assessment. The two datasets were compared in terms of their spatial coverage of actual parking conditions within the study area, using aerial imagery, Google Street View, and Google Earth as references.

Figure 5.1 shows the overall study area around the TUM main campus and compares the coverage of parking areas derived from the TIAS segmentation results with those labeled as TrafficArea in the CityGML dataset. When comparing Figure 5.1 (b) and (c), it becomes clear that the parking areas detected by TIAS are more scattered throughout the region, with many polygons appearing inside residential blocks. This suggests that the TIAS segmentation is capable of identifying private parking spaces that belong to the residents of these buildings, where access is usually restricted.

Although such private parking areas within courtyards are not directly related to cyclist safety on public streets, this result demonstrates the ability of TIAS to detect even non-public parking spaces. A few false detections were also found in the TIAS-derived dataset, where rectangular objects resembling vehicles were mistakenly identified as cars, resulting in the creation of false parking polygons. However, since these errors occurred away from streets, they are not expected to influence visibility for road users.

In contrast, the CityGML dataset mainly includes parking spaces located along streets. While it does not cover private areas, it provides consistent and complete information on public parking spaces. The gaps seen along certain streets reflect real-world conditions, for instance, driveways or entrances leading to private parking areas where street parking is not allowed.

Figure 5.1 (d) illustrates the overlap between both datasets. The missing parking areas in the TIAS results are likely due to the absence of vehicles at the time the aerial imagery was captured, which could depend on factors such as the time of day. Some streets, such as Heßstraße in the upper-left part of the figure, show a high overlap between the datasets, while others, like Arcisstraße running vertically through the middle, have few TIAS detections even though most of the street is designated for public parking. Conversely, smaller

streets in the bottom-left area marked in red circle show several TIAS-detected parking areas that are not represented in the CityGML data.

A closer examination of the actual parking situation on one of these streets, Richard-Wagner-Straße, is presented in Figure 5.2.

(a) Google Earth view of the study area surrounding TUM.

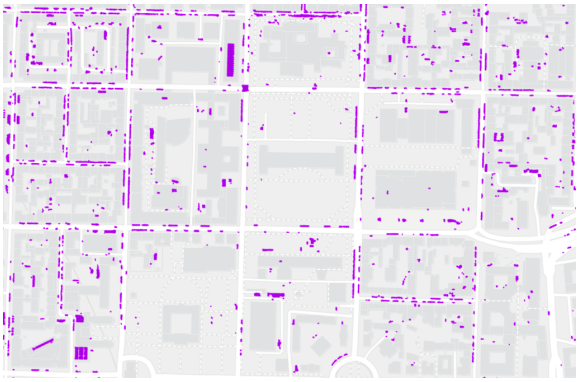

(b) TIAS-derived parking polygons (purple).

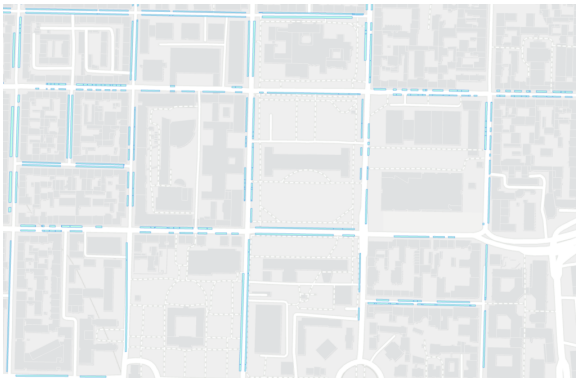

(c) CityGML lane model parking areas (light blue).

(d) Combined TIAS and CityGML parking data. The overlap of TIAS segmentation results and CityGML parking is marked black.

Figure 5.1: Comparison of parking representations in TIAS and CityGML datasets in the study area around the TUM main campus

The Rheinstraße study area showed a similar pattern: the main street (Rheinstraße) had a high coverage of parking areas in the CityGML dataset, while the intersecting, mostly residential streets were not included. It should be noted, however, that the CityGML dataset used for the TUMDOT project was primarily created with a focus on Rheinstraße itself. As a result, the completeness of the data is likely higher for this main street than for the surrounding side streets. Figure 5.3 illustrates an example of the parking situation around an intersection on Rheinstraße. The light blue areas represent the CityGML lane model

Figure 5.2: Actual parking situation seen in Richard-Wagner-Straße.

features classified as “parking,” while the purple polygons correspond to the TIAS-derived parking areas. The parking along the main street (Rheinstraße, west–east direction) is well captured by the CityGML data. In contrast, the crossing street (Mainzerstraße, north–south direction) contains no designated parking areas in the CityGML dataset. The TIAS-derived data, however, demonstrate a broader coverage on both streets, although some segments are missing, likely due to the absence of parked vehicles in the imagery used during the detection process, or the influence of shading and the presence of trees, which made it difficult to cpature clear view of parked vehicles.

(a) Google Earth view of the intersection.

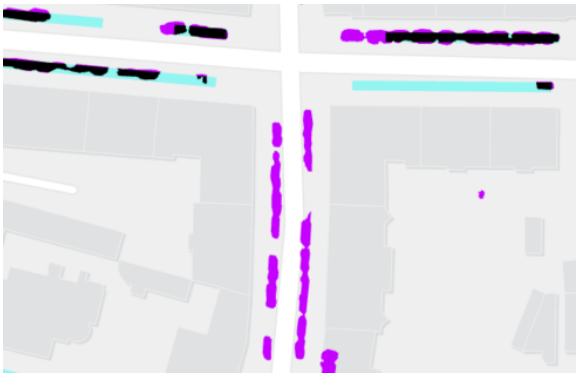

(b) Combined TIAS and CityGML parking data. The area marked light blue is the CityGML-derived TrafficArea for parking, purple is TIAS semgmentation results, and black is the overlap between the two datasets.

Figure 5.3: Comparison of parking representations in TIAS and CityGML datasets around the intersection of Rheinstraße and Mainzerstraße.

5.2 Intervisibility Analysis Results

This section presents the results of the intervisibility analyses conducted for two study areas: Rheinstraße and the area surrounding TUM. The hook collision type was further divided into right-hook and left-hook patterns to examine distinct sight obstruction characteristics in greater detail. For each study area and collision type, the number of conflict points, visibility outcomes by obstruction category, and the spatial identification of obstruction locations are described and analyzed.

5.2.1 Hook Visibility in Rheinstraße

In this area, a total of 16 right-hook conflict points were identified as shown in Figure 5.4.

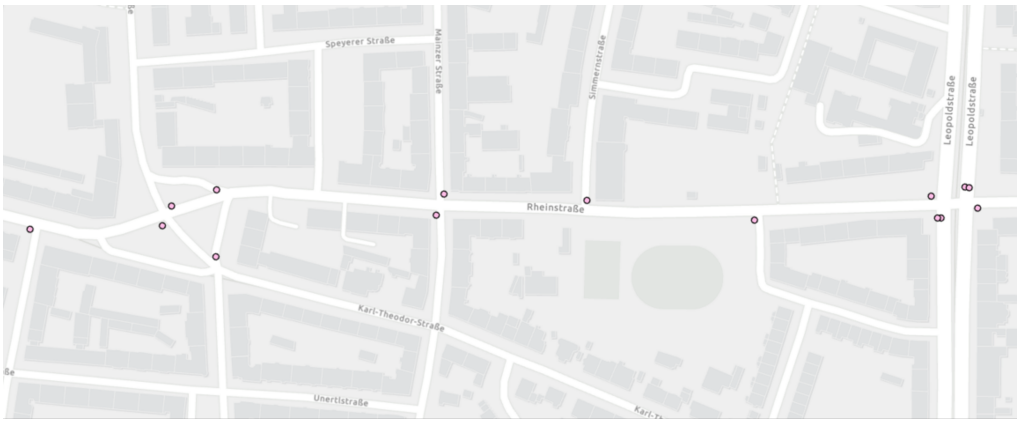

(a) Right-hook conflict points

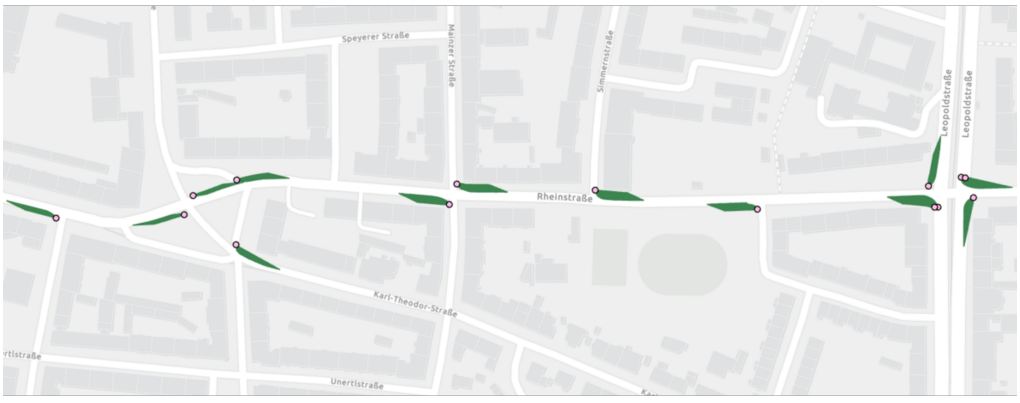

(b) Left-hook conflict points

Figure 5.4: (a) Right-hook conflict points identified on Rheinstraße. (b) Generated sight lines marked green connecting observer (driver) and target (cyclist) points

Out of the right-hook points, eight were located at signalized intersections and seven at

non-signalized intersections. The category-based blockage rates indicated that obstructions caused by vegetation and buildings were not observed for the right-hook collision type. The impact of city furniture on visibility ranged from 0% to 3%, with an average blockage rate of approximately 1%. In contrast, parked vehicles showed a more profound influence: eight out of the 16 identified conflict points were affected by their presence, with blockage rates reaching up to 86% and an overall mean of 30%. The summary by category is shown in Table 5.1.

Conflict point	Vegetation BR	Building BR	City furniture BR	Parking BR
1	0%	0%	0%	85.5%
2	0%	0%	0%	80.9%
3	0%	0%	1.4%	62.0%
4	0%	0%	1.4%	57.5%
5	0%	0%	1.5%	48.7%
6	0%	0%	0.7%	40.5%
7	0%	0%	0%	40.1%
8	0%	0%	0.8%	33.7%
9	0%	0%	0%	0%
10	0%	0%	0%	0%
11	0%	0%	0%	0%
12	0%	0%	0%	0%
13	0%	0%	0%	0%
14	0%	0%	3.0%	0%
15	0%	0%	0%	0%
16	0%	0%	0%	0%

Table 5.1: Right-hook collision Blocked Rate (BR) percentages for vegetation, building, city furniture, parking, and street space (S1, S2) obstructions at each conflict point.

Overall, parked vehicles represented the primary source of visibility obstruction, followed by city furniture, which had only a marginal effect. The *Line of Sight* analysis further revealed that among city furniture, visibility reductions were solely caused by traffic light poles positioned along the roadside at signalized intersections. The Figure 5.11 illustrates a traffic light pole responsible for the highest blockage rate (3%) among city furniture objects. The pink plane represents the dense cluster of sight lines connecting drivers' and cyclists' paths at 0.5 m intervals, appearing as a solid surface due to their high density. A close examination of the quantified results together with the street-view imagery shown in the images of the intersection indicates that a 3% blockage rate caused by the traffic light pole shown in Figure 5.5 (a) does not cause a substantial visibility impairment likely to result in drivers overlooking adjacent cyclists solely due to the presence of the pole. This could indicate that a single object that has 3% or lower, with the absence of other visibility blockage factors,

contribute little to actual intervisibility impairment.

In contrast, a closer inspection of the parked vehicle results revealed that a single feature could produce a much higher blockage rate—up to 86% in this case (Figure 5.6). It should be noted that each parked vehicle feature in this study often represents multiple vehicles parked longitudinally rather than a single car.

(a) Line of Sight (LoS) analysis showing the traffic light pole (black) obstructing cyclists' visibility.

(b) Street-view image of the same intersection showing the real-world position of the pole.

Figure 5.5: Comparison between 3D LoS analysis and street-view imagery illustrating the minor visibility obstruction (3%) caused by a traffic light pole at a signalized intersection on Rheinstraße.

The impact of parked vehicles on the mutual visibility between cyclists and motorists was observed only in cases where a roadside parking lane was located between the cycling lane and the driveway. When the average blockage rate was calculated for conflicts under these conditions, it reached as high as 56%.

As for left-hook conflict, 14 left-hook conflict points were identified (Figure 5.7), of which seven were located at signalized intersections and seven at non-signalized intersections. The category-based blockage rates indicated that obstructions caused by vegetation and buildings were not observed for the left-hook collision type, which was similar to the results of the right-hook collision analysis. The impact of city furniture on visibility ranged from 0% to 5.1%, with an average blockage rate of approximately 1.3%. In contrast, parked vehicles showed a more pronounced influence: four out of the 14 identified conflict points were affected by their presence, with blockage rates reaching up to 53.6% and an overall mean of 9.4%. The blocked rate is summarized in Table 5.2

The obstruction identification results exhibited a pattern similar to that of the right-hook type. Within the city furniture category, sight blockages were primarily caused by traffic light poles and electricity poles, with the highest blockage value from an individual feature reaching 5.0%, indicating a relatively minor impact. In contrast, the obstruction caused by parked vehicles was considerably more significant. A detailed examination of individual

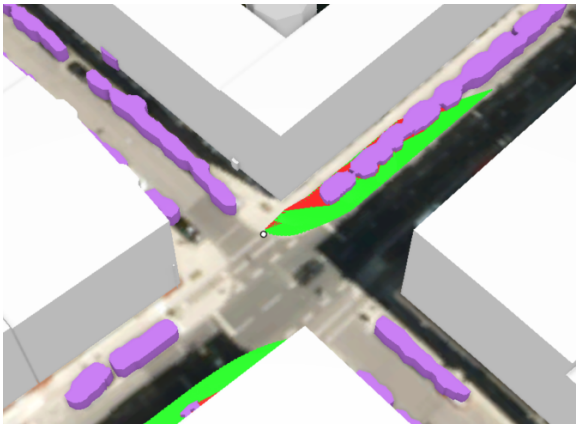

(a) Line of Sight (LoS) analysis showing the parked vehicle area (purple) obstructing visibility at the intersection. The unobstructed sight lines are green, and the sections invisible from driver's viewpoint is marked red.

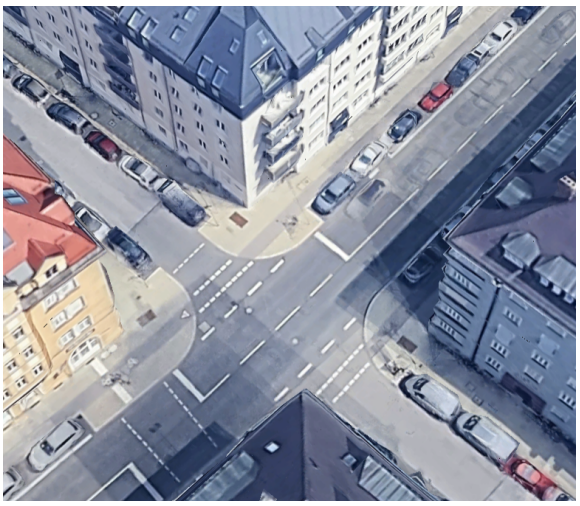

(b) Aerial view of the same intersection showing the actual parked vehicles along the curb.

Figure 5.6: Comparison between 3D LoS analysis and aerial imagery showing a parked vehicle feature responsible for the highest blockage rate (87%) among all analyzed points on Rheinstraße.

cases revealed that, as in the right-hook pattern, parked vehicles had a pronounced effect when the parking lane was situated between the driveway and the cycling lane. In such configurations, left-turning drivers had limited visibility of cyclists positioned behind the parked vehicles. The specific situation for this case is illustrated in Figure 5.8, where the blue line represents the driver's left-turning path, the pink line indicates the cycling path, and the purple objects denote parked vehicles.

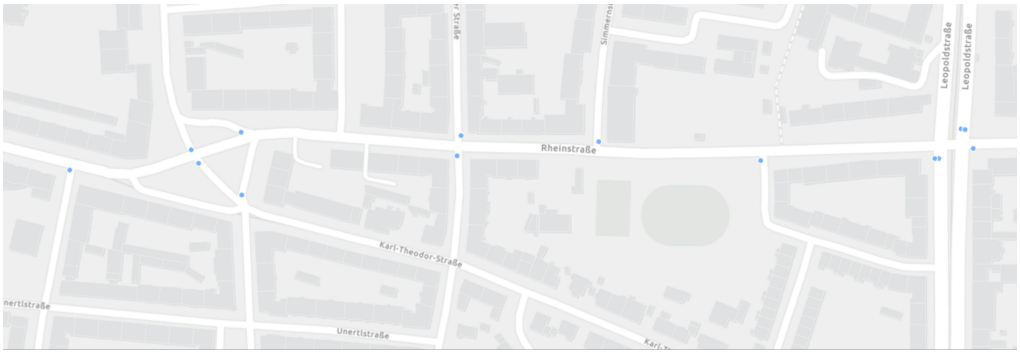

(a) Right-hook conflict points

(b) Left-hook conflict points

Figure 5.7: (a) Left-hook conflict points identified on Rheinstraße. (b) Generated sight lines marked light-green connecting observer (driver) and target (cyclist) point

Conflict point	Vegetation BR	Building BR	City furniture BR	Parking BR	S1 BR	S2 BR
1	0%	0%	0%	53.6%	0%	53.6%
2	0%	0%	0%	43.8%	0%	43.8%
3	0%	0%	4.7%	27.0%	4.7%	31.7%
4	0%	0%	0%	7.7%	0%	7.7%
5	0%	0%	5.1%	0%	5.1%	5.1%
6	0%	0%	4.7%	0%	4.7%	4.7%
7	0%	0%	1.6%	0%	1.6%	1.6%
8	0%	0%	1.5%	0%	1.5%	1.5%
9	0%	0%	0%	0%	0%	0%
10	0%	0%	0%	0%	0%	0%
11	0%	0%	0%	0%	0%	0%
12	0%	0%	0%	0%	0%	0%
13	0%	0%	0%	0%	0%	0%
14	0%	0%	0%	0%	0%	0%

Table 5.2: Left-hook collision Blocked Rate (BR) percentages for vegetation, building, city furniture, parking, and street space obstructions (S1, S2) at each conflict point.

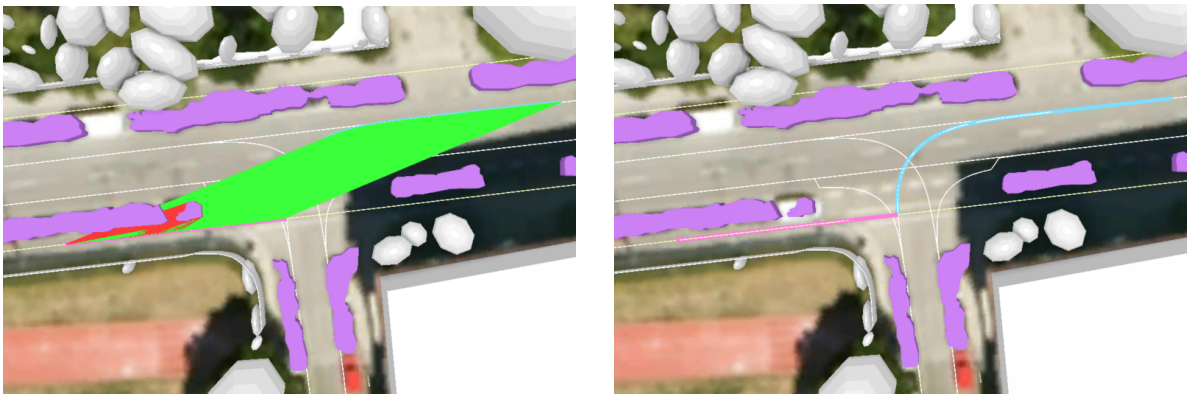

(a) LoS analysis highlighting the obstruction caused by parked vehicles between the driving and cycling lanes. The unobstructed sight lines are green, and the sections invisible from driver's viewpoint is marked red.

(b) Path configuration showing the driver's left-turning trajectory (blue), the cycling path (pink), and parked vehicles (purple).

Figure 5.8: Example of a left-hook conflict scenario in Rheinstraße where parked vehicles obstruct the driver's visibility of cyclists approaching from behind.

5.3 Crossing Collision in Rheinstraße

A total of nine crossing-type conflict points were identified in this study area (Figure 5.9). Since signalized intersections were assumed to resolve such conflicts by temporally assigning

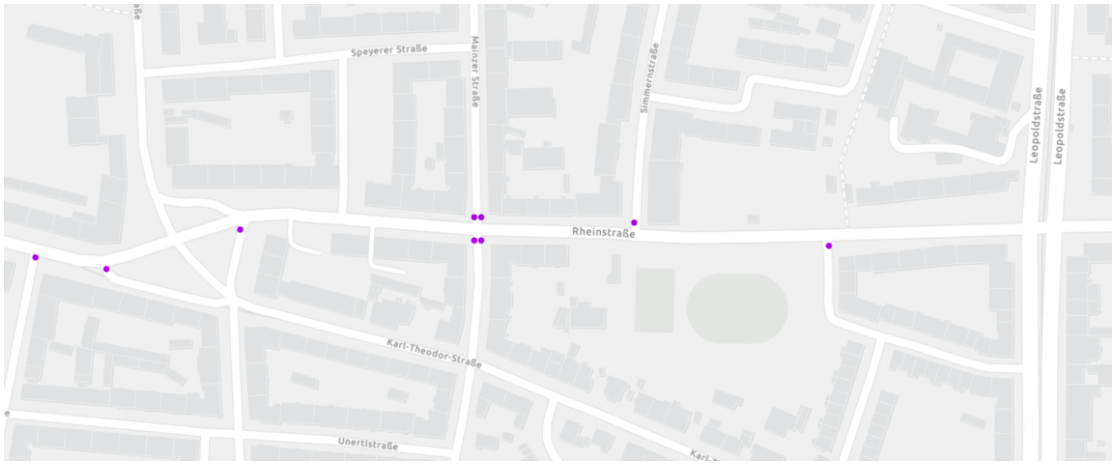

Figure 5.9: Crossing conflict points (pink) identified on Rheinstraße.

priority, only conflict points located within non-signalized intersections were included in this analysis. Furthermore, due to the absence of explicit cycling lane data on minor roads, where cyclists and motorists share the same roadway, the analysis focused exclusively on cases where drivers on minor roads needed to observe cyclists approaching from the left or right before crossing the main road. Sight lines generated from the resulting conflict point sorting is shown in Figure 5.10

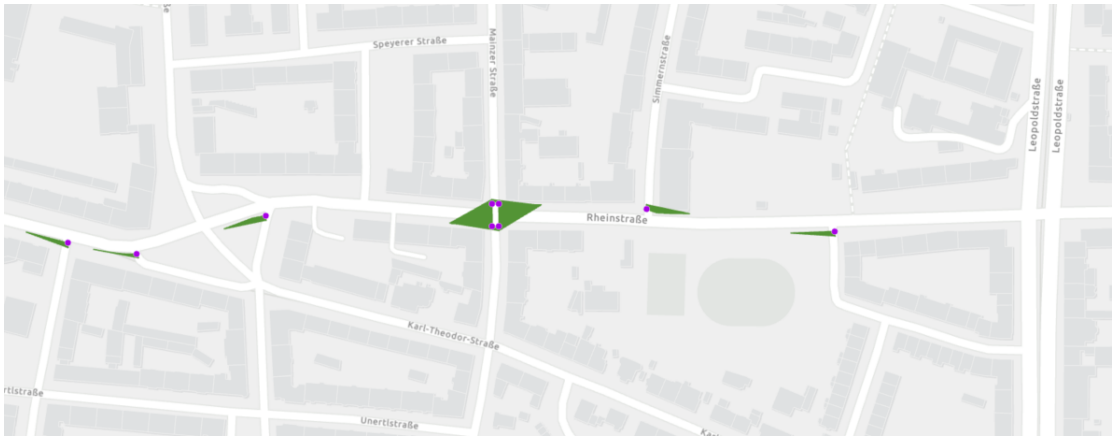

Figure 5.10: sight lines (green) generated for crossing conflicts on Rheinstraße.

Out of the nine identified conflicts, three were affected by ground-level obstructions. Buildings contributed to one of these conflicts, with a blockage rate of 59.3%, while parked

vehicles affected the other two, with blockage rates of 16.9% and 67.8%, respectively. Table 5.3 shows the summary of blocked rate by category.

Conflict point	Vegetation BR	Building BR	City furniture BR	Parking BR
1	0%	0%	0%	67.8%
2	0%	0%	0%	16.9%
3	0%	0%	0%	0%
4	0%	0%	0%	0%
5	0%	0%	0%	0%
6	0%	0%	0%	0%
7	0%	0%	0%	0%
8	0%	59.3%	0%	0%
9	0%	0%	0%	0%

Table 5.3: Crossing-collision Blocked Rate (BR) percentages for vegetation, building, city furniture, and parking obstructions at each conflict point.

The Figure 5.11 illustrates a case in which a building located at the corner of a T-shaped intersection obstructed the driver's view of a cyclist approaching from the right.

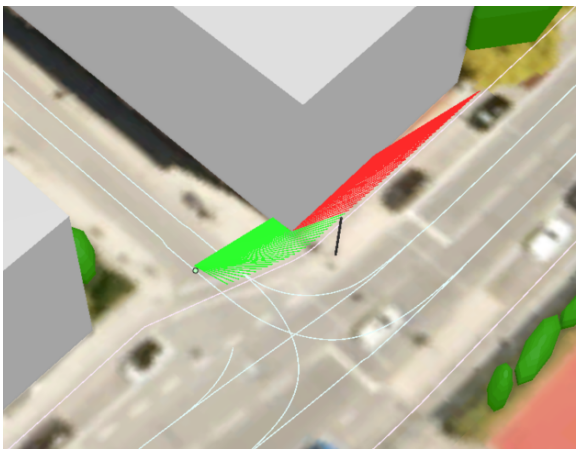

(a) LoS analysis showing a building corner (gray) obstructing the driver's visibility of an approaching cyclist. Green lines and red lines indicate visible and invisible sections of sight lines respectively

(b) Aerial view of the same intersection illustrating the obstruction at the corner building.

Figure 5.11: Example of a crossing-type visibility obstruction in Rheinstraße, where a building corner limits the driver's sight of an approaching cyclist.

The two conflicts caused by parked vehicles are illustrated in Figure 5.12. In case (a), a driver entering Rheinstraße from the north was unable to see 67.8% of the trajectory of cyclists approaching from the west due to parked vehicles obstructing the view in front of the intersection. In case (b), a driver entering the main street from the opposite side

experienced a similar issue, as 16.9% of the cycling path was concealed by parked vehicles.

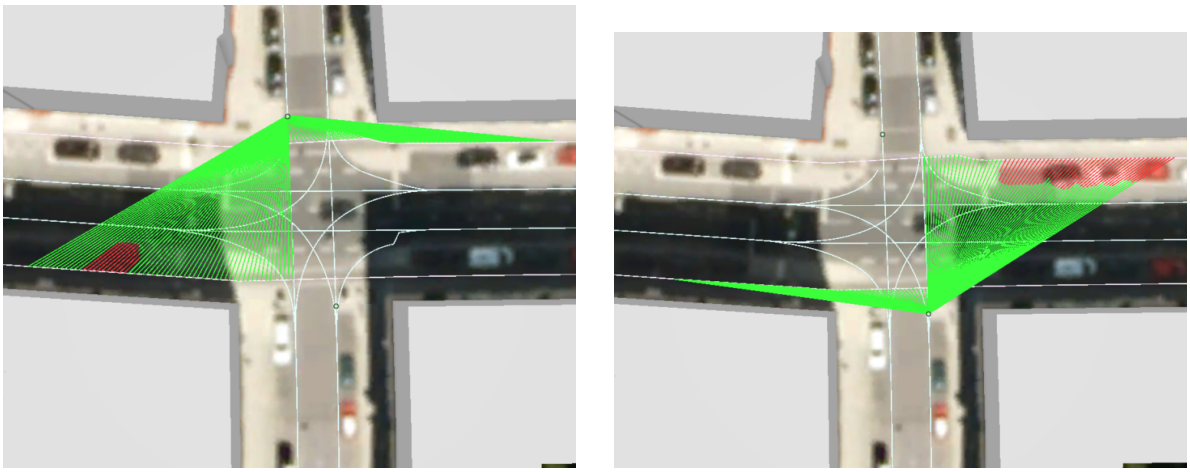

(a) Driver entering from the north; 67.8% of cyclists' path obstructed by parked vehicles.

(b) Driver entering from the opposite side; 16.9% of cyclists' path obstructed by parked vehicles.

Figure 5.12: Examples of crossing-type visibility obstructions in Rheinstraße caused by parked vehicles blocking cyclists approaching from the sides.

5.3.1 Hook Visibility around TUM

In the study area surrounding TUM, a total of 11 right-hook conflicts were identified. Among these, six were located within signalized intersections and three within non-signalized intersections. The remaining two occurred on segments leading to signalized intersections, where the number of driving lanes increased from one to two. In these cases, drivers used a dedicated right-turn lane, and the lane-change path intersected with a cycling lane continuing straight through the upcoming intersection. Although the spatial coverage of the TUM study area was larger than that of Rheinstraße, the number of identified conflicts was not significantly higher. This was mainly due to the presence of numerous one-way streets, which reduced potential conflict occurrences, as well as missing connections, particularly among bikeways, in the lane model dataset. The identified conflict points and their associated sight lines are shown in Figure 5.13

The category-based results indicated that at two intersections, trees influenced intervisibility by 22.9% and 7.2%, respectively. Parked vehicles were involved in five right-hook conflicts, with blockage rates ranging from 18.9% to 76.7%, while city furniture and buildings did not contribute to any observable obstructions. Table 5.4 shows by-category results at each right-hook conflict.

A closer examination of the impact of individual elements on visibility revealed that the obstruction attributed to trees was unlikely to occur in reality, or at least not to the same

Figure 5.13: Conflict points (pink) and sight lines (light-green) generated for right-hook conflicts around TUM

extent. This discrepancy arose from the use of 3D tree assets in the Solitary Vegetation model. As described in the previous chapter, tree geometries were approximated based on crown diameter and tree type; however, the height of the lower boundary of the crown did not necessarily correspond to actual conditions. The comparison between the ArcGIS scene and the Google Street View image in Figure 5.14 shows that the pink points, representing cyclists' viewpoints, appear to intersect the tree crown. In contrast, in reality, the branches are elevated high enough not to obstruct the bikeway.

As observed in the Rheinstraße study area, cases where parking affected intervisibility occurred when the parking lane was situated between the cycling path and the driving path.

As for the left-hook analysis, a total of eight left-hook conflict points were identified in this area, of which three were located at signalized intersections and five at non-signalized intersections (Figure 5.15). The category-based results indicated that at two intersections, trees influenced intervisibility by 24.5% and 8.0%, respectively. However, it was the same biking path that was interfered with directly by the low tree crown. Therefore, the actual effects of the tree at these locations are considered neither significant nor any at all. Parked vehicles were involved in five left-hook conflicts, with blockage rates ranging from 25.2% to 37.3%, while city furniture and buildings did not contribute to any observable obstructions. The sumamry table is in Table 5.5

Conflict point	Vegetation BR	Building BR	City furniture BR	Parking BR
1	0%	0%	0%	76.6%
2	7.2%	0%	0%	51.3%
3	0%	0%	0%	27.2%
4	22.9%	0%	0%	19.9%
5	0%	0%	0%	18.9%
6	0%	0%	0%	0%
7	0%	0%	0%	0%
8	0%	0%	0%	0%
9	0%	0%	0%	0%
10	0%	0%	0%	0%
11	0%	0%	0%	0%

Table 5.4: Right-hook Blocked Rate (BR) percentages for vegetation, building, city furniture, and parking obstructions at each conflict point.

Conflict point	Vegetation BR	Building BR	City furniture BR	Parking BR
1	24.5%	0%	0%	37.3%
2	0%	0%	0%	34.3%
3	8.0%	0%	0%	25.2%
4	0%	0%	0%	0%
5	0%	0%	0%	0%
6	0%	0%	0%	0%
7	0%	0%	0%	0%

Table 5.5: Left-hook Blocked Rate (BR) percentages for vegetation, building, city furniture, and parking obstructions at each conflict point.

(a) ArcGIS 3D scene showing cyclists' viewpoints (pink points) intersecting the tree crown geometry.

(b) Google Street View image showing that actual tree branches are elevated above the cyclists' line of sight.

Figure 5.14: Comparison of 3D vegetation model and real-world conditions on Theresienstraße, illustrating discrepancies in modeled tree crown height.

5.3.2 Crossing Collision around TUM

A total of four crossing-type conflict points were analyzed in this study area (Figure 5.16). The conflict points available for analysis were quite few due to a lack of completeness in the bikeway data. Additionally, the presence of signalized intersections was familiar, which helps prevent this type of collision; therefore, the number of conflicts to be investigated was relatively small. The category-wise analysis revealed that city furniture and buildings did not affect the visibility of the four conflicts. Only at a conflict point were their sight lines blocked by a tree and parked vehicles. The category summary is in Table 5.6

Conflict point	Vegetation BR	Building BR	City furniture BR	Parking BR
1	3.3%	0%	0%	33.0%
2	0%	0%	0%	0%
3	0%	0%	0%	0%
4	0%	0%	0%	0%

Table 5.6: Crossing-collision Blocked Rate (BR) percentages for vegetation, building, city furniture, and parking obstructions

A closer look based on the identified obstruction ID revealed that, as with the case of hook accident types, a tree near the corner of an intersection had a low crown that interfered with the bikeway, causing a blockage value of 3.3%, while two parked vehicle obstacles located

Figure 5.15: Conflict points (light-blue) and sight lines (light-green) generated for left-hook conflicts around TUM

on the same roadside blocked 10% and 23% of sight lines, respectively (Figure 5.17).

Figure 5.16: Conflict points (light-orange) and sight lines (orange) generated for left-hook conflicts around TUM

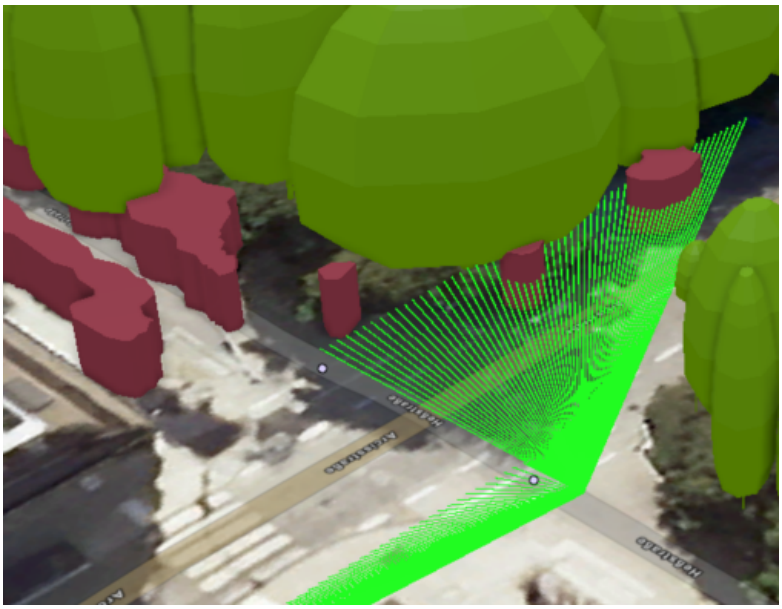

Figure 5.17: LoS analysis at a TUM-area intersection showing a low tree crown obstructing the cyclists' line of sight (green sightlines) and additional parked vehicles contributing to visibility blockage.

6 Discussion and Limitation

The

6.1 Potential of Scalability

The applied methodology required extensive modifications to the original dataset due to incompleteness issues that were not inherent to the CityGML format itself but rather specific to the dataset produced within the originating project. Some data limitations still necessitated manual interventions; therefore, a fully automated visibility evaluation was not achieved. However, it is worth noting that full automation would be feasible, depending on the selected metric or indicator. In this study, the methodology was designed to include a degree of manual inspection to ensure data accuracy and analytical reliability.

The methodology developed to quantify intervisibility at intersections was guided by the principle of utilizing the original, readily available data with minimal preprocessing that requires manual inspection. However, the input line data, which formed the foundation of this study for extracting the paths of both cyclists and drivers, contained missing connections and, in some cases, incorrect labels. This required careful inspection during data preparation and import into the 3D scene. As discussed in the implementation section, the absence of cycling path data on mixed-use streets was particularly evident in both study areas. This issue arises from the fact that road usage labels in the dataset were primarily based on car drivability and the physical capacity for bicycles, rather than on actual cycling behavior. Consequently, routes frequently used by cyclists were not represented in the original CityGML transportation data. In cities like Munich, where many side and minor streets lack dedicated cycling lanes, it would be highly beneficial to include bikeable paths in the dataset explicitly.

In addition to the lack of data on certain streets, path discontinuities made it challenging to use the dataset in its original form. The upstream extraction method employed in this study relied on the assumption that each path could be continuously traced as long as it was spatially connected. However, discontinuities, particularly in cycling paths, were observed in both study areas and had to be manually corrected to ensure proper network connectivity. The supplement of data using OpenStreetMap as an alternative data source was attempted

but the dataset also had missing components although the spatial accuracy in the positions of the cycling lanes within streets was good when they were examined referring to aerial images. Therefore the additional cycling lane datasets can be used as complementary data, but not to replace CityGML lane model for cycling lanes.

Additionally, the lane model in its original form did not include road usage labels or speed information in its attribute table. Although these data were available in the original GML file, making the semantic information accessible required manual verification, as discussed in the data preparation section. At present, no reliable method has been identified to automatically detect the hierarchical level at which these specific generic attributes of interests are stored. Therefore, the use of an alternative data processing tool or a customized programming approach may be necessary to efficiently extract and manage these semantic attributes. As mentioned earlier, the labeling of road usage was not always accurate, and manual corrections were made where necessary. Similarly, some inconsistencies were found between the speed information in the lane model and the data derived from OpenStreetMap. However, verifying the actual speed limits proved difficult, as ground-truth information was often unavailable or unclear in Google Street View. When reliable reference data is available, it is recommended to validate the speed attributes in the CityGML dataset to ensure consistency and accuracy.

Furthermore, the standard CityGML Transportation Module does not include information on traffic priority rules or right-of-way regulations at intersections. Visibility analyses based on sight triangles require a clear definition of such hierarchical relationships to determine which users must yield and which have priority. For signalized intersections, it would also be ideal to include signal control logic to identify which paths have simultaneous green phases and which conflicts are regulated by traffic lights. Public availability of traffic signal sequences and patterns as digital data is not clear, although it is possible to observe the patterns at the intersection of interest.

Regarding the limitations of the implemented workflow, the process of automatically classifying conflict points according to car–bicycle accident patterns was not successful. Automating the identification of right-hook, left-hook, or crossing conflicts could potentially be achieved by analyzing the spatial relationships between the connected paths, specifically, whether the cycling path joins the driving path from the right or left. Another limitation was related to the upstream tracing algorithm, which terminated tracing when a path split and could not determine which branch to follow. Simple decision rules could be implemented to automate this selection process. As a result, the upstream paths extracted using the arcpy scripts occasionally produced incomplete segments, and in some cases, the tracing direction was incorrect. Verification against the original OpenDrive data would be necessary to confirm whether the directional information associated with each segment was accurate. Due to

these issues, manual editing of the extracted segments generated by the script was required.

By addressing these challenges and utilizing high-quality input data, the potential for complete automation, and thus for efficient, city-wide application, is considerably high. Although there remains room for improvement, the inclusion of two study sites, Rheinstraße and the area around TUM, was beneficial, as it allowed verification of the developed method's applicability across two distinct locations with datasets originating from independent projects.

In contrast to the limited scalability of CityGML-derived datasets, the TIAS segmentation model demonstrated strong potential as a foundation for large-scale visibility studies. Using manually annotated aerial images from the TIAS dataset as input, the trained model can classify road environments according to their functional use, from which primary and secondary parking spaces can be extracted. This implies that, as long as high-resolution DOP aerial imagery is available, the analysis can be scaled flexibly—even up to the national level.

6.2 Evaluation of CityGML and TIAS Data for 3D Visibility Analysis

The suitability of the CityGML Transportation Module for visibility analysis has been discussed previously. This section focuses on the use of CityGML data to represent obstructions such as vegetation, buildings, and city furniture. Subsequently, the effectiveness of TIAS-based parking data in representing roadside parked vehicles as visibility obstructions is examined.

6.2.1 CityGML Roadside Objects

The missing components in previous visibility studies, such as semantic labeling, identification of the exact locations of sight-obstructing factors, and quantification of the extent to which they block visibility, were effectively addressed through the use of CityGML data. In terms of attribute table operations, including extraction, calculation, joining, and aggregation across multiple geoprocessing steps, CityGML demonstrated strong usability for deriving numerical visibility indicators in a systematic workflow. In this regard, CityGML as a data format proved to be a practical foundation for the visibility analysis framework developed in this research.

However, a closer examination of the results concerning the impact of different object types on visibility highlights the importance of both precise geometric representation and data completeness. Regarding vegetation geometry, the original data from the Solitary Vegetation project used in this thesis were collected using airborne imagery captured from an

altitude of approximately 480 meters [Münzinger et al. 2022]. While the crown shapes of trees were accurately represented, trunk diameters were estimated as 4% of the crown diameter. Comparisons with Google Street View imagery, however, indicate that several trees have significantly smaller trunk diameters than those estimated in the dataset. Additionally, some bushes were misclassified as trees, a discrepancy attributable to the data collection method. Because the dataset was derived from airborne imagery that primarily captured the canopy from above, the detailed geometry beneath the crown was not detected. For instance, several bushes near Königsplatz were classified as trees, which substantially affected ground-level visibility at adjacent intersections, as shown in Figure 6.1.

(a) 3D representation of vegetation around Königsplatz in the CityGML dataset.

(b) Street-view image showing the actual vegetation height and structure.

Figure 6.1: Comparison between the CityGML vegetation model and real-world conditions at Königsplatz, illustrating misclassification of low bushes as trees.

Although seasonal variations in leaf density affect the transparency of vegetation, the thin trunk representation, as shown in Figure 6.1(a), does not fully capture its actual potential to obstruct visibility. Compared with LiDAR-based methods, which are increasingly common and capable of representing fine details such as foliage and stem curvature [Kilani et al. 2021; Ma et al. 2022], the geometric representation of vegetation in CityGML still has considerable limitations.

City furniture elements such as traffic signal poles, light poles, and signs were found to cause minor visibility obstructions in some of the analyzed conflict cases. However, the overall extent of their impact was minimal and, in most cases, negligible. This observation is reasonable, as such installations are typically designed and positioned to avoid hinder-

ing the visibility of road users. The City Furniture module itself, however, encompasses a broader range of urban objects, including advertisements, benches, fences, and other street elements. Although none of these additional object types contributed to sight obstructions in the present study, they may influence visibility in other urban contexts if the study area were expanded.

Regarding building objects, the level of detail (LoD) used in this thesis was LoD2, determined by data availability. However, since the required level of detail for analyzing mutual visibility between cyclists and motorists is primarily relevant at ground level, higher detail representations, such as roof structures in LoD3, do not significantly influence the results. Therefore, the building dataset employed in this study can be considered fully adequate and well-suited for the intended visibility analysis.

6.2.2 TIAS

The TIAS parking segmentation results in comparison with the CityGML TrafficArea–labeled parking data were described in the section section 5.1. In addition to the advantages and limitations outlined above, another important factor to consider when using TIAS data for road visibility analysis is the timing and conditions under which the data were captured. TIAS imagery is collected during daytime, whereas nighttime conditions often differ significantly, particularly due to increased roadside parking as residents return home and park along the streets. Moreover, parking conditions are highly dependent on the specific moment of image acquisition. While TIAS has the advantage over CityGML in capturing roads with parking as a secondary usage, thus reflecting more realistic parking situations, CityGML better represents officially designated primary parking areas. The quality of TIAS data is also affected by tree canopies, as it is derived from aerial imagery, which makes it challenging to detect ground-level parking conditions without additional complementary data sources. Ideally, the parking situation should be derived from both TIAS and CityGML datasets, as they can complement each other by compensating for the limitations and missing information present in each source.

Additionally, the approach employed to represent parked vehicles in three dimensions was oversimplified, as it relied solely on extruded polygons. A more realistic representation could be generated by modeling 3D rectangular prisms based on the vehicle footprints, better approximating the actual shapes of cars. Incorporating realistic longitudinal gaps between parked vehicles would further enhance accuracy, as such gaps allow road users to perceive each other's presence even when partially obscured by parked vehicles. A more realistic representation could be achieved by using vehicle detection data directly, instead of parking area data. As demonstrated in recent work by Bahmanyar et al. (2025), deep-learning-based

vehicle detection could provide output data, which can be a valuable foundation for visibility study.

Another potential advantage of integrating TIAS data into the 3D scene is its ability to distinguish the orientation of roadside parking spaces, whether parallel, diagonal, or perpendicular to the adjacent street, during the data generation process. This information is not yet semantically or geometrically represented in CityGML. Incorporating parking orientation data would significantly enrich CityGML datasets, enabling the generation of virtual 3D parked vehicle objects arranged more realistically.

6.3 Validation of Results

Since the framework of this study relies on automated geoprocessing methods that integrate multiple data sources, it is essential to assess whether the obtained results accurately reflect real-world road conditions. This validation is partially addressed in the results section, particularly when examining the high blockage rates caused by vegetation in the study area around TUM. As visibility- or sight-related measurement data are not readily available, validation is primarily conducted through comparisons with aerial imagery, Google Maps Street View, and Google Earth. At both study sites, locations exhibiting high blockage rates are visually inspected to determine whether the identified obstructions correspond to actual roadside elements such as parked vehicles, vegetation, street furniture, or buildings.

While the inspections and qualitative validation indicate that the results are plausible, their quantitative accuracy and reliability remain subject to certain limitations. In the absence of ground-truth visibility measurements, it is difficult to draw precise conclusions about the validity of the results. For instance, even though traffic light poles at a right-hook intersection were found to block approximately 3% of visibility, such obstruction may not significantly affect intervisibility. Consequently, the extent to which cyclists are exposed to visibility-related risks cannot yet be conclusively determined.

6.4 Establishing Safety Assessment Steps

The applied procedure in this study does not follow the well-established methodologies commonly used in road visibility and safety research. Conventional approaches typically measure available sight distance using LiDAR-acquired data and similar technologies, focusing primarily on the distance a driver can see ahead along the roadway. Furthermore, due to the limited number of bicycle-centered studies, cyclist visibility has rarely been examined in depth. Therefore, the approach developed and applied in this thesis should be regarded as exploratory and subject to further verification and validation.

Driving and cycling maneuvers near potential conflict areas inherently involve complex sequences of actions, and the resulting sightlines between cyclists and drivers depend strongly on case-specific conditions. For instance, the driver's eye height varies depending on the vehicle type; although a height of 1.2 m was assumed in this thesis, it can exceed 2 m for drivers of large trucks or buses. Moreover, the applied approach did not constrain the horizontal viewing angle, whereas in reality, both drivers and cyclists have limited horizontal fields of view. Drivers also rely on side and rear-view mirrors to detect cyclists overtaking from behind when turning, which provides perspectives different from those determined solely by eye-level positions.

The employed visibility assessment approach yielded structured and sufficiently precise outputs, providing valuable insights for road safety evaluation. However, the available tools, Intervisibility and Line of Sight, imposed certain analytical limitations. Ideally, visibility assessment should be conducted over continuous lines or planes rather than discrete points representing eye-level positions, as used in this study. Although the chosen point interval was relatively small, the reliability of the results would increase if visibility were modeled continuously. The tools used in this thesis accept only sightlines as input, which must be derived from observer and target points, thus restricting the analysis to discrete geometries.

Moreover, incorporating vertical elements of visibility would enhance realism. In practice, cyclists do not necessarily make eye contact with drivers but instead perceive the presence of vehicles through visible portions of their bodies. Therefore, it is more relevant to determine whether any vertical section of the vehicle is visible to the cyclist's line of sight. This consideration aligns with the German sight triangle regulation, which specifies that the sight triangle should remain unobstructed between heights of 0.8 m and 2.5 m.

6.5 Integration of TIAS dataset into CityGML Transport Module

The direct integration of TIAS segmentation results into the CityGML Transportation module, particularly the TrafficArea and TrafficSpace features, was only partially successful. This limitation mainly occurred because the FME CityGML writer does not yet support version 3.0. Although attribute values could be modified within the existing dataset, creating a new CityGML file that includes the updated information for this module was not possible.

If this function were available, the parking information could be stored under genericAttribute, similar to how lane type and speed attributes are managed. The planned approach was to add a new attribute field dedicated to parking information in the TrafficArea layer, named "ParkingUsage." Since public parking areas along major roads are already represented in the original CityGML data, these features could inherit the attribute value "Primary."

For all non-parking features, overlaps with TIAS data were tested. If a TIAS polygon overlapped with a road feature, the overlapping section was extracted as an independent feature and assigned "Secondary" to its ParkingUsage attribute. Features that neither overlapped with TIAS data nor had an original parking type were classified as "Non_parking." The overall concept and procedure are illustrated in Figure 6.2 and the FME Workbench workflow is shown in Figure 6.3.

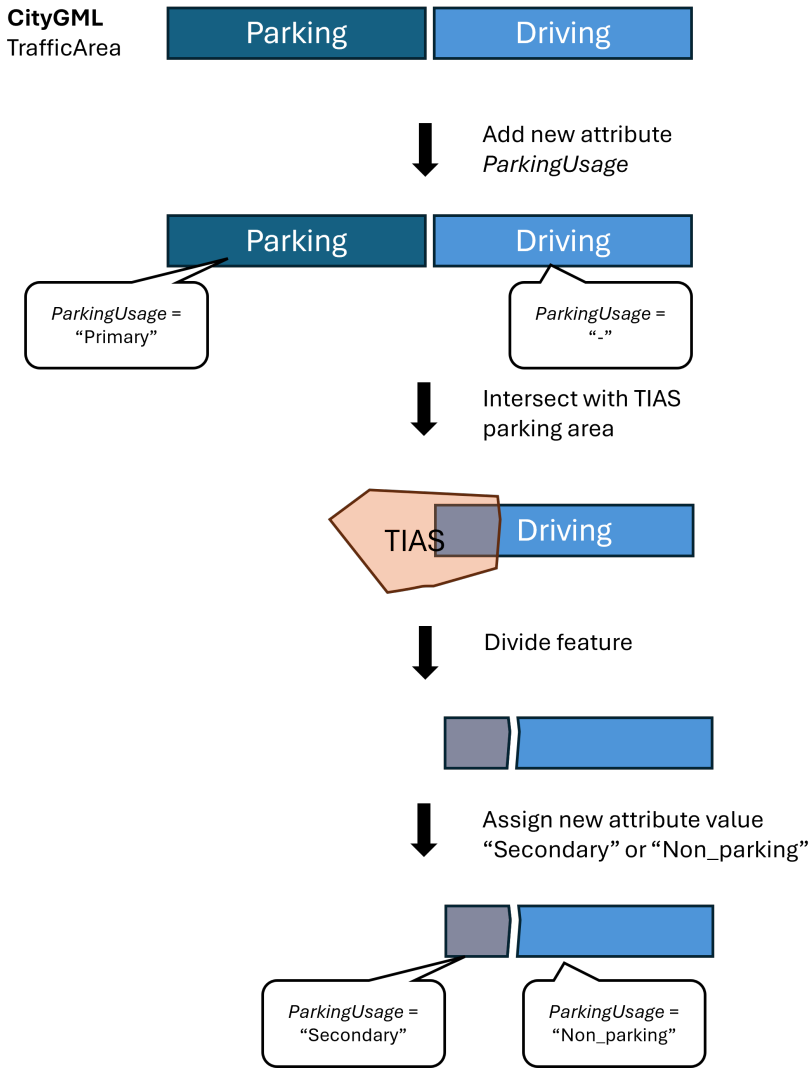

Figure 6.2: Concept of assigning the ParkingUsage attribute based on TIAS overlaps and existing CityGML lane information.

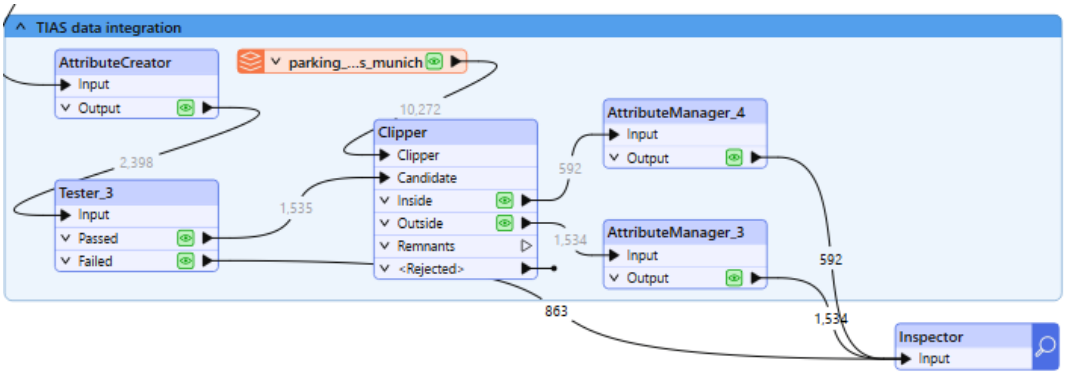

Figure 6.3: FME Workbench workflow for TIAS data integration into the CityGML Transport module.

6.6 Further Work

As this project had an exploratory nature, especially in terms of new types of input data and quantification methodologies, verifying the output reliability in comparison with actual traffic accident statistics would be reasonable. Unlike previous research, which targeted already problematic accident hotspots, this thesis aims to identify locations that may require closer attention. The validity of the approach should first be confirmed with the actual data.

In terms of the quantification method, no distinction was made between blockages occurring near the conflict point and those farther away from it. Early detection of another road user's presence is crucial for accident prevention; however, obstructions immediately before the conflict point can lead to more severe accidents, as not all users consistently maintain attention to others well in advance of the conflict zone. In this thesis, all sightlines were weighted equally regardless of their spatial distance from the corresponding conflict point. Nevertheless, the analysis could yield more meaningful insights if greater weight were assigned to blockages occurring closer to the conflict point.

Another potential area for improvement or future application involves the inclusion of dynamic obstruction elements, such as moving vehicles in urban traffic. Due to their transient nature, it is challenging to design a visibility study that comprehensively quantifies the effects of moving vehicles. However, it may be feasible to simulate specific real-world traffic scenarios, such as queues of vehicles at a red light, that temporarily obstruct the visibility of other road users approaching or entering an intersection.

7 Conclusion

This paper constructs and implements a systematic framework for three-dimensional visibility analysis to evaluate the safety of bicycle users at urban intersections, utilizing urban models with semantic information and parking data. By integrating CityGML 3.0 and TIAS data within a GIS-based environment, the study presents a reproducible workflow that achieves both geometric accuracy and semantic depth, overcoming the limitations of conventional "motorist-centric" and static visibility studies.

Analysis results confirmed that the proposed methodology can quantify intervisibility between cyclists and motorists and identify urban elements that obstruct sightlines. Notably, parked vehicles emerged as the most significant factor reducing visibility among obstructions, while impacts from buildings, vegetation, and street furniture were relatively minor. These results suggest the need to incorporate temporary or semi-permanent roadside elements into traffic safety analyses in urban environments with high-density on-street parking.

Furthermore, this study clarified the potential and challenges of automated, city-scale visibility assessment using CityGML and TIAS data. While CityGML demonstrated high effectiveness in representing permanent roadside elements and semantic analysis, manual corrections were required for missing connections and incomplete attributes. TIAS data complemented the virtual road environment by reflecting actual parking conditions; however, its reliance on aerial imagery highlighted limitations in temporal constraints.

Although requiring certain preprocessing steps, the workflow developed in this paper demonstrated the feasibility of scalable visibility assessment across multiple intersections, paving the way for city-wide applications. Furthermore, this methodology provides a foundation for future extensions, such as dynamic traffic scenarios, real-time data, and object-level behavior analysis.

Ultimately, this research contributes to the advancement of data-driven urban safety analysis, including for bicycle users. By linking 3D urban data with semantic information and visibility metrics, it provides insights for urban planners, transportation engineers, and policymakers in designing safer, more visible street environments. Future challenges include incorporating dynamic elements, further advancing automation of processing, and validating the approach through comparison with actual traffic accident data.

Bibliography

Allgemeiner Deutscher Fahrrad-Club (ADFC). (2024). Adfc-fahrradklima-test 2024: Das sind die ergebnisse [Nationwide survey by ADFC assessing the cycling friendliness of German cities and municipalities]. Retrieved August 24, 2025, from https://fahrradklima-test.adfc.de/

Allgemeiner Deutscher Fahrrad-Club (ADFC) e.V. (2020). Innorad factsheet: Kreuzungen [Factsheet from the InnoRAD project by the German Cyclists' Association (ADFC)]. Retrieved August 26, 2025, from https://www.adfc.de/fileadmin/user_upload/Expertenbereich/Politik_und_Verwaltung/Download/adfc_innorad_kreuzungen_web.pdf

Association for Standardisation of Automation and Measuring Systems (ASAM). (2025). Opendrive [ASAM OpenDRIVE standard for the logical description of road networks]. Retrieved August 26, 2025, from https://www.asam.net/standards/detail/opendrive/

Bahmanyar, R., Hellekes, J., Mühlhaus, M., Gstaiger, V., & Kurz, F. (2025). Traffic pattern analysis at urban intersections through vehicle detection in aerial imagery. *ISPRS Annals of the Photogrammetry, Remote Sensing and Spatial Information Sciences*, *X-G-2025*, 151–158. https://doi.org/10.5194/isprs-annals-X-G-2025-151-2025

Bassani, M., Grasso, N., & Piras, M. (2015). 3d gis based evaluation of the available sight distance to assess safety of urban roads. *The International Archives of the Photogrammetry, Remote Sensing and Spatial Information Sciences*, *XL-3/W3*, 137–143. https://doi.org/10.5194/isprsarchives-XL-3-W3-137-2015

Bayerische Vermessungsverwaltung. (2025). Opendata – kostenfreie geodaten der bayerischen vermessungsverwaltung [Accessed from the official Bavarian OpenData portal]. Retrieved October 13, 2025, from https://geodaten.bayern.de/opengeodata/OpenDataDetail.html?pn=lod2

Beil, C., Ilic, M., Keler, A., & Kolbe, T. H. (2024). Automatically evaluating the service quality of bicycle paths based on semantic 3d city models. In T. H. Kolbe, A. Donaubauer, & C. Beil (Eds.), *Recent advances in 3d geoinformation science* (pp. 75–92). Springer Nature Switzerland. https://doi.org/10.1007/978-3-031-43699-4{\textunderscore}5

Beil, C., Ruhdorfer, R., Coduro, T., & Kolbe, T. H. (2020). Detailed streetspace modelling for multiple applications: Discussions on the proposed citygml 3.0 transportation model. *ISPRS International Journal of Geo-Information*, *9*(10), 603. https://doi.org/10.3390/ijgi9100603

Biljecki, F., Stoter, J., Ledoux, H., Zlatanova, S., & Çöltekin, A. (2015). Applications of 3d city models: State of the art review. *ISPRS International Journal of Geo-Information*, *4*(4), 2842–2889. https://doi.org/10.3390/ijgi4042842

Brown, L., Morris, A., Thomas, P., Ekambaram, K., Margaritis, D., Davidse, R., Usami, D. S., Robibaro, M., Persia, L., Buttler, I., Ziakopoulos, A., Theofilatos, A., Yannis, G., Martin, A., & Wadji, F. (2021). Investigation of accidents involving powered two wheelers and bicycles - a european in-depth study. *Journal of safety research*, *76*, 135–145. https://doi.org/10.1016/j.jsr.2020.12.015

Buch, T. S., & Jensen, S. U. (2017). Incidents between straight-ahead cyclists and right-turning motor vehicles at signalised junctions. *Accident; analysis and prevention*, *105*, 44–51. https://doi.org/10.1016/j.aap.2016.07.035

Copenhagenize Design Company. (2025). Copenhagenize index – the index of bicycle-friendly cities [Information page about the Copenhagenize Index ranking methodology for bicycle-friendly cities]. Retrieved August 24, 2025, from https://copenhagenizeindex.eu/about/the-index/

Cumming, B. (2012). Conflict path analysis: Analysing and managing the cyclist–driver interface [Presented at the AITPM National Conference, 2012. Record available via TRID: The TRIS and ITRD Database.]. *Proceedings of the Australian Institute of Traffic Planning and Management (AITPM) National Conference*, 1–16. https://trid.trb.org/view/12457768

Ding, H., Sze, N. N., Guo, Y., & Li, H. (2021). Role of exposure in bicycle safety analysis: Effect of cycle path choice. *Accident; analysis and prevention*, *153*, 106014. https://doi.org/10.1016/j.aap.2021.106014

Esri. (2025). Line of sight (3d analyst) — arcgis pro documentation [ArcGIS 3D Analyst tool documentation for line-of-sight analysis]. Retrieved August 26, 2025, from https://pro.arcgis.com/en/pro-app/latest/tool-reference/3d-analyst/line-of-sight.htm

Forschungsgesellschaft für Straßen- und Verkehrswesen (FGSV). (2001). *R-fgü: Richtlinien für die anlage und ausstattung von fußgängerüberwegen (guidelines for the design and equipment of pedestrian crossings)* [Technical guideline on pedestrian crossing design, including placement criteria, markings, signage, and lighting requirements]. Retrieved August 25, 2025, from https://www.fgsv-verlag.de/pub/media/pdf/252.v.pdf

Forschungsgesellschaft für Straßen- und Verkehrswesen (FGSV). (2012). *Ral 2012: Richtlinien für die anlage von landstraßen (guidelines for the design of rural roads)* [Normative stan-

dard covering rural road layout, cross-section design, alignment, and safety-related geometric parameters]. Retrieved August 25, 2025, from https://fgsv-verlag.de/pub/media/pdf/201.i.pdf

Forschungsgesellschaft für Straßen- und Verkehrswesen (FGSV). (2006). *Rast 06: Richtlinien für die anlage von stadtstraßen (guidelines for the design of urban roads)* [Comprehensive guideline defining the design principles, functional classification, cross-sections, and intersection design for urban road networks]. Retrieved August 25, 2025, from https://www.fgsv-verlag.de/pub/media/pdf/200.i.pdf

Forschungsgesellschaft für Straßen- und Verkehrswesen (FGSV), Working Group Highway Design. (2008). *Raa: Richtlinien für die anlage von autobahnen (guidelines for the design of motorways)* [Guideline specifying standards for motorway design including horizontal and vertical alignment, junctions, cross-sections, and equipment]. Retrieved August 25, 2025, from https://fgsv-verlag.de/pub/media/pdf/202_E_PDF.v.pdf

Gargoum, S. A., & Karsten, L. (2021). Virtual assessment of sight distance limitations using lidar technology: Automated obstruction detection and classification. *Automation in Construction*, *125*, 103579. https://doi.org/10.1016/j.autcon.2021.103579

Gehring, D. B. (2018). *Bikeability – index für dresden* [Master's Thesis]. Technische Universität Dresden. Retrieved August 24, 2025, from https://tud.qucosa.de/api/qucosa%3A30317/attachment/ATT-0/

Gesamtverband der Deutschen Versicherungswirtschaft e.V. (GDV), Unfallforschung der Versicherer (UDV). (2025). Pressemitteilungen [Press releases by the German Insurance Association's Accident Research Division (UDV)]. Retrieved August 26, 2025, from https://www.udv.de/udv/presse/82282/pressemitteilungen

González-Gómez, K., & Castro, M. (2019). Evaluating pedestrians' safety on urban intersections: A visibility analysis. *Sustainability*, *11*(23), 6630. https://doi.org/10.3390/su11236630

González-Gómez, K., López-Cuervo Medina, S., & Castro, M. (2021). Assessment of intersection conflicts between riders and pedestrians using a gis-based framework and portable lidar. *GIScience & Remote Sensing*, *58*(4), 587–602. https://doi.org/10.1080/15481603.2021.1920199

González-Gómez, K., Rollins, D. K., & Castro, M. (2022). Modeling urban road scenarios to evaluate intersection visibility. *Sustainability*, *14*(1), 354. https://doi.org/10.3390/su14010354

Harkort, L., Walker, B. B., & Lakes, T. (2023). Spatiotemporal patterns of cyclist collisions in germany: Variations in frequency, severity of injury, and type of collision in 2019. *Applied Spatial Analysis and Policy*, *16*(1), 209–228. https://doi.org/10.1007/s12061-022-09476-w

Hudde, A. (2022). The unequal cycling boom in germany. *Journal of Transport Geography*, *98*, 103244. https://doi.org/10.1016/j.jtrangeo.2021.103244

Jung, J., Olsen, M. J., Hurwitz, D. S., Kashani, A. G., & Buker, K. (2018). 3d virtual intersection sight distance analysis using lidar data. *Transportation Research Part C: Emerging Technologies*, *86*, 563–579. https://doi.org/10.1016/j.trc.2017.12.004

Kahlmeier, S., Boig, E. A., Castro, A., Smeds, E., Benvenuti, F., Eriksson, U., Iacorossi, F., Nieuwenhuijsen, M. J., Panis, L. I., Rojas-Rueda, D., Wegener, S., & de Nazelle, A. (2021). Assessing the policy environment for active mobility in cities—development and feasibility of the pasta cycling and walking policy environment score. *International Journal of Environmental Research and Public Health*, *18*(3). https://doi.org/10.3390/ijerph18030986

Kazemzadeh, K., Laureshyn, A., Winslott Hiselius, L., & Ronchi, E. (2020). Expanding the scope of the bicycle level-of-service concept: A review of the literature. *Sustainability*, *12*(7). https://doi.org/10.3390/su12072944

Kilani, O., Gouda, M., Weiß, J., & El-Basyouny, K. (2021). Safety assessment of urban intersection sight distance using mobile lidar data. *Sustainability*, *13*(16), 9259. https://doi.org/10.3390/su13169259

Kurokawa. (2023). *Plateau technical document no. 0057, version 1.0* (tech. rep.) (Technical documentation from the PLATEAU project on 3D urban data development in Japan). Ministry of Land, Infrastructure, Transport and Tourism (MLIT), PLATEAU Project. Retrieved August 25, 2025, from https://www.mlit.go.jp/plateau/file/libraries/doc/plateau_tech_doc_0057_ver01.pdf

Kutzner, T., Chaturvedi, K., & Kolbe, T. H. (2020). Citygml 3.0: New functions open up new applications. *PFG – Journal of Photogrammetry, Remote Sensing and Geoinformation Science*, *88*(1), 43–61. https://doi.org/10.1007/s41064-020-00095-z

Labetski, A., van Gerwen, S., Tamminga, G., Ledoux, H., & Stoter, J. (2018). A proposal for an improved transportation model in citygml. *The International Archives of the Photogrammetry, Remote Sensing and Spatial Information Sciences*, *XLII-4/W10*, 89–96. https://doi.org/10.5194/isprs-archives-XLII-4-W10-89-2018

Li, W., Arzoumanidis, L., Matijevic, J., Mustafa, D. M., Rottmann, P., Haunert, J.-H., & Dehbi, Y. (2024). Safety assessment of cycling routes in urban environments. *The International Archives of the Photogrammetry, Remote Sensing and Spatial Information Sciences*, *XLVIII-4/W10-2024*, 125–130. https://doi.org/10.5194/isprs-archives-XLVIII-4-W10-2024-125-2024

Ma, Y., Zheng, Y., Wong, Y. D., Easa, S., & Cheng, J. (2022). A virtual procedure for real-time monitoring of intervisibility between conflicting agents at intersections using point

cloud and trajectory data. *Transportation Research Part C: Emerging Technologies*, *134*, 103486. https://doi.org/10.1016/j.trc.2021.103486

Magyari, Z., & Koren, C. (2018). Visibility indicators for intersection safety investigation. *International Conferences on Traffic and Transport Engineering - ICTTE Belgrade*. https://doi.org/10.1016/j.jtrangeo.2021.103244

Morrison, C. N., Thompson, J., Kondo, M. C., & Beck, B. (2019). On-road bicycle lane types, roadway characteristics, and risks for bicycle crashes. *Accident Analysis & Prevention*, *123*, 123–131. https://doi.org/https://doi.org/10.1016/j.aap.2018.11.017

Münzinger, M., Prechtel, N., & Behnisch, M. (2022). Mapping the urban forest in detail: From lidar point clouds to 3d tree models. *Urban Forestry & Urban Greening*, *74*, 127637. https://doi.org/10.1016/j.ufug.2022.127637

Omer Malak and European Cyclists' Federation (ECF). (2022). *Geometric design parameters for cycling infrastructure* [Technical guideline published by the European Cyclists' Federation (ECF)]. Retrieved October 7, 2025, from https://bicycleinfrastructuremanuals.com/manuals7/ECF-Geometric-Design-Parameters-for-Cycling-Infrastructure-2022.pdf

PLATEAU Project, Ministry of Land, Infrastructure, Transport and Tourism (MLIT). (2025). Topic 3 – citygml: How to use [2/4] [Tutorial from the PLATEAU project on the use of CityGML data in Japan]. Retrieved August 25, 2025, from https://www.mlit.go.jp/plateau/learning/tpc03-2/

Rauch, F., Henry, C., Mühlhaus, M., Kurz, F., Hellekes, J., & Merkle, N. (2025). Large-scale mapping of urban parking from aerial images: A case study in berlin, germany. *The International Archives of the Photogrammetry, Remote Sensing and Spatial Information Sciences*, *XLVIII-4/W16-2025*, 83–89. https://doi.org/10.5194/isprs-archives-XLVIII-4-W16-2025-83-2025

Saeidi Razavi, R., & Furth, P. G. (2021). Risk to bicyclists in a separated path from left turns across multiple lanes: A case for protected-only left turns. *Transportation Research Record*, *2675*(10), 174–183. https://doi.org/10.1177/03611981211010789

Schmid-Querg, J., Keler, A., & Grigoropoulos, G. (2021). The munich bikeability index: A practical approach for measuring urban bikeability. *Sustainability*, *13*(1), 428. https://doi.org/10.3390/su13010428

Schröter, B., Hantschel, S., Huber, S., & Gerike, R. (2023). Determinants of bicycle crashes at urban signalized intersections. *Journal of safety research*, *87*, 132–142. https://doi.org/10.1016/j.jsr.2023.09.011

Schwab, B., Beil, C., & Kolbe, T. H. (2020). Spatio-semantic road space modeling for vehicle–pedestrian simulation to test automated driving systems. *Sustainability*, *12*(9), 3799. https://doi.org/10.3390/su12093799

Statistisches Bundesamt (Destatis). (2022). *Kraftrad- und fahrradunfälle im straßenverkehr 2021* (Official report on motorcycle and bicycle accidents in road traffic, published by the Federal Statistical Office of Germany (Destatis)). Retrieved August 26, 2025, from https://www.destatis.de/DE/Themen/Gesellschaft-Umwelt/Verkehrsunfaelle/Publikationen/Downloads-Verkehrsunfaelle/unfaelle-zweirad-5462408217004.pdf

StVO2Go. (2022). Sichtdreiecke im straßenverkehr berechnen: Der komplette guide 2go [Online guide on calculating visibility triangles in road traffic, published by StVO2Go]. Retrieved August 25, 2025, from https://www.stvo2go.de/sichtdreiecke-berechnen/

Tan, Y., Liang, Y., & Zhu, J. (2023). Citygml in the integration of bim and the gis: Challenges and opportunities. *Buildings*, *13*(7), 1758. https://doi.org/10.3390/buildings13071758

Technical University of Munich (TUM). (2025). Tum2twin [Research initiative aiming to create a comprehensive digital twin of the TUM campus]. Retrieved August 26, 2025, from https://tum2t.win/

Technical University of Munich (TUM), Chair of Geoinformatics. (2025). R:trån – opendrive to citygml converter [Software developed at TUM for converting OpenDRIVE data to CityGML format]. Retrieved August 26, 2025, from https://www.asg.ed.tum.de/en/gis/software/rtron/

Technical University of Munich (TUM), Chair of Geoinformatics. (2023). Road2citygml3 – version 1.0 documentation [Open-source tool developed at TUM for converting road data to CityGML 3.0 format]. Retrieved August 25, 2025, from https://tum-gis.github.io/road2citygml3/

Technical University of Munich (TUM), Chair of Traffic Engineering and Control. (2025). Tumdot-muc: Trajectories from urban multimodal drone observations of traffic – munich [Open dataset containing multimodal traffic trajectories recorded by drones in Munich in October 2022; available under CC BY-NC 4.0 license. For methodological details, see Kutsch, A., Margreiter, M. & Bogenberger, K. (2024): *TUMDOT–MUC: Data Collection and Processing of Multimodal Trajectories Collected by Aerial Drones*. Data Science for Transportation, 6, 15. https://doi.org/10.1007/s42421-024-00101-5]. Retrieved August 26, 2025, from https://www.mos.ed.tum.de/en/vt/research/datasets/tumdot-muc/

Unfallforschung der Versicherer (UDV). (2013). *Unfälle zwischen abbiegenden kfz und radfahrern* [Study on accidents between turning motor vehicles and cyclists, published by UDV (GDV)]. Gesamtverband der Deutschen Versicherungswirtschaft e.V. (GDV). https://publish.fid-move.qucosa.de/detailansicht/?tx_dlf%5Bid%5D=https%3A%2F%2Fpublish.fid-move.qucosa.de%2Fapi%2Fqucosa%253A74759%2Fmets

Useche, S. A., Alonso, F., Boyko, A., Buyvol, P., Castañeda, I., Cendales, B., Cervantes, A., Echiburu, T., Faus, M., Feitosa, Z., Gene, J., Gonzalez-Marin, A., Gonzalez, V., Gnap,

J., Ibrahim, M. K., Janstrup, K. H., Javadinejad, A., Makarova, I., McIlroy, R., … Montoro, L. (2022). Cross-culturally approaching the cycling behaviour questionnaire (cbq): Evidence from 19 countries. *Transportation Research Part F: Traffic Psychology and Behaviour*, *91*, 386–400. https://doi.org/https://doi.org/10.1016/j.trf.2022.10.025

Wang, Y., & Nihan, N. L. (2004). Estimating the risk of collisions between bicycles and motor vehicles at signalized intersections. *Accident Analysis and Prevention*, *36*(3), 313–321. https://doi.org/10.1016/S0001-4575(03)00009-5

Warner, J., Hurwitz, D. S., Monsere, C. M., & Fleskes, K. (2017). A simulator-based analysis of engineering treatments for right-hook bicycle crashes at signalized intersections. *Accident; analysis and prevention*, *104*, 46–57. https://doi.org/10.1016/j.aap.2017.04.021

Wysocki, O., Schwab, B., Biswanath, M. K., Greza, M., Zhang, Q., Zhu, J., Froech, T., Heeramaglore, M., Hijazi, I., Kanna, K., Pechinger, M., Chen, Z., Sun, Y., Segura, A. R., Xu, Z., AbdelGafar, O., Mehranfar, M., Yeshwanth, C., Liu, Y.-C., … Jutzi, B. (2025). Tum2twin: Introducing the large-scale multimodal urban digital twin benchmark dataset. https://arxiv.org/pdf/2505.07396